Direct and inverse electromagnetic scattering problems for bi-anisotropic media*

IOP Publishing Inverse Problems

Inverse Problems **35** (2019) 124001 (27pp) https://doi.org/10.1088/1361-6420/ab382d

Direct and inverse electromagnetic scattering problems for bi-anisotropic media*

Dinh-Liem Nguyen

Department of Mathematics, Kansas State University, Manhattan, KS 66506, United States of America

E-mail: dlnguyen@ksu.edu

Received 23 March 2019, revised 9 July 2019
Accepted for publication 2 August 2019
Published 24 October 2019

Abstract

This paper is concerned with the direct and inverse scattering of time-harmonic electromagnetic waves from bi-anisotropic media. For the direct problem, we establish an integro-differential equation formulation, its Fredholm property, and the uniqueness of a weak solution. Using this integro-differential formulation we study a fast spectral Galerkin method for the numerical solution to the direct problem. Numerical examples are presented and convergence of the spectral method is proved via Gårding estimates for (strongly singular) integro-differential equations. We solve the inverse problem of recovering bi-anisotropic scatterers from far-field data using orthogonality sampling methods. These methods aim to construct imaging functionals which are robust to noise, computationally cheap, and require data for only one or a few incident fields. We provide some theoretical analysis as well as numerical simulations for the proposed imaging functionals.

Keywords: bi-anisotropic media, fast numerical solution, orthogonality sampling, electromagnetic scattering, inverse electromagnetic scattering, integro-differential equation

(Some figures may appear in colour only in the online journal)

1. Introduction

In this paper we study theoretical analysis and computational algorithms for both direct and inverse electromagnetic scattering problems for inhomogeneous bi-anisotropic media. This study is motivated by potential applications of electromagnetic scattering from complex

* This paper is dedicated to the memory of Professor Armin Lechleiter.

media (e.g. bi-anisotropic media, chiral media) in optics and metamaterials, as well as nondestructive evaluations [21, 26, 33]. The topic of electromagnetic propagation and scattering in complex media has recently received an increasing amount of interest from mathematicians. Theoretical analysis for the direct problem in both the time domain and frequency domain can be found in [1, 3, 4, 10, 11, 31, 32, 36, 37]. We particularly refer to the book [37] for an account of the most recent mathematical results on complex media electromagnetics. As can be seen in [37], and to our knowledge, there have been only a limited number of papers addressing numerical analysis and computational algorithms for direct and inverse scattering problems for electromagnetic complex media. For the direct problem, we refer to [40, 41] for finite element methods to solve simplified two-dimensional problems. Numerical analysis of the full Maxwell's equations can be found in [2, 30] for the case of chiral media.

The study for the direct problem in this paper can be considered as an extension of the results in [15, 18, 30]. More precisely, we extend the integro-differential formulation and its Fredholm property from the case of isotropic magnetic media [18] and the Drude–Born–Fedorov model for chiral media [15] to the case of bi-anisotropic media. The spectral Galerkin method framework for solving the direct problem is extended from the results of [30]. Besides the typical complications from full Maxwell's equations in complex media, the main theoretical issue in the integro-differential formulation lies in proving the Gårding inequalities for strongly singular integro-differential operators involving matrix-valued coefficients. In addition, we establish a result on the uniqueness of a weak solution to the direct problem, which leads to the existence and uniqueness of the solution for the direct problem and the integro-differential formulation. We note that our results for both direct and inverse problems in this paper can be applicable to other simpler cases of inhomogeneous (complex) media such as bi-isotropic, chiral, anisotropic or magnetic media.

For the inverse scattering problem, although there are large numbers of studies on reconstruction algorithms for inverse electromagnetic scattering problems, results for the case of electromagnetic complex media are quite limited and mainly focus on theoretical issues. We refer to [5, 6, 14, 23, 27, 28, 39] for uniqueness results. Some results on numerical reconstructions can be found in [7, 8, 14] for simplified two dimensional problems. The shape identification problem for inverse scattering for full Maxwell's equations in chiral media has been studied in [15, 29]. These papers studied the factorization method of Kirsch [19] as a tool for the imaging of bounded and periodic chiral scatterers.

In this paper we study the orthogonality sampling method (OSM) introduced by Potthast in [35] to solve the inverse scattering problem. More precisely, we extend the OSM analyzed for the sound-soft acoustic case in [35] to full Maxwell equations in bi-anisotropic media. The integro-differential formulation derived for the direct problem plays an important role in this extension. We provide some theoretical analysis for the imaging functionals derived from the OSM as well as numerical simulations, demonstrating the efficiency of these imaging functionals.

The OSM also belongs to a class of sampling methods including the linear sampling method, the factorization method, the probe and singular source method, see [9, 19, 34] and the references therein. The main advantage of the OSM compared with these sampling methods is that it requires scattering data for only one or a few incident waves and its stability can be justified easily. However, its mathematical basis is not as complete as those of the sampling methods mentioned above. We also refer to [17, 22, 24] for recently developed sampling methods, sharing similar features to the OSM.

The paper is organized as follows. The direct problem and its basic setup are presented in section 2. In section 3 we establish the integro-differential formulation for the direct problem and prove its Fredholm property. Section 4 contains a proof for the uniqueness of a weak

solution to the direct problem, which also implies the existence of a weak solution thanks to the Fredholm property. A fast spectral method, its convergence analysis as well as numerical examples are presented in section 5. The inverse problem and OSMs are studied in section 6. Finally, section 7 is dedicated to numerical simulations of OSMs for the inverse problem.

2. Direct problem formulation

We consider the scattering of time-harmonic electromagnetic waves at a positive frequency ω from a bi-anisotropic medium. Let $\mathbf{E}$ be the electric field and $\mathbf{H}$ be the magnetic field while $\mathbf{B}$ and $\mathbf{D}$ are respectively the magnetic induction and the electric displacement. The fields are described by Maxwell's equations (with no free charge and current density)

$$\operatorname{curl}\mathbf{E} - \mathrm{i}\omega\mathbf{B} = 0, \quad \operatorname{curl}\mathbf{H} + \mathrm{i}\omega\mathbf{D} = 0, \quad \text{in } \mathbb{R}^3. \tag{1}$$

The constitutive relations for bi-anisotropic media are described as [20, 25]

$$\mathbf{B} = \mu\mathbf{H} + \xi\sqrt{\varepsilon_0\mu_0}\,\mathbf{E}, \quad \mathbf{D} = \varepsilon\mathbf{E} + \overline{\xi}\sqrt{\varepsilon_0\mu_0}\,\mathbf{H}. \tag{2}$$

Here ε and μ are respectively the electric permittivity and the magnetic permeability of the medium. The parameter ξ is typically described as $\xi = \chi + \mathrm{i}\kappa$ where χ is the chirality parameter and κ is the non-reciprocity parameter of the medium. These parameters are assumed to be matrix-valued bounded functions.

Suppose that the bi-anisotropic medium is inhomogeneous and occupies a bounded domain Ω while the medium outside of Ω is assumed to be homogeneous. This means that there exists positive constants ε_0 and μ_0 such that $\varepsilon = \varepsilon_0 I_3$, $\mu = \mu_0 I_3$, and $\xi = 0 I_3$ in $\mathbb{R}^3 \setminus \overline{\Omega}$ (I_3 is the 3×3 identity matrix), see figure 1 for a schematic of the scattering problem. The relative material parameters and the wave number are defined by

$$\varepsilon_{\mathrm{r}} = \varepsilon/\varepsilon_0, \quad \mu_{\mathrm{r}} = \mu/\mu_0, \quad k = \omega\sqrt{\varepsilon_0\mu_0}.$$

Rescaling the fields by $\mathbf{E} = \sqrt{\varepsilon_0}\,\mathbf{E}$ and $\mathbf{H} = \sqrt{\mu_0}\,\mathbf{H}$ (without changing notation), and then substituting (2) in (1) we have

$$\operatorname{curl}\mathbf{E} - \mathrm{i}k(\mu_{\mathrm{r}}\mathbf{H} + \xi\mathbf{E}) = 0, \quad \operatorname{curl}\mathbf{H} + \mathrm{i}k(\varepsilon_{\mathrm{r}}\mathbf{E} + \overline{\xi}\mathbf{H}) = 0, \quad \text{in } \mathbb{R}^3. \tag{3}$$

Now we eliminate $\mathbf{H}$ from (3) to obtain

$$\operatorname{curl}[\mu_{\mathrm{r}}^{-1}\operatorname{curl}\mathbf{E}] + \mathrm{i}k[\overline{\xi}\mu_{\mathrm{r}}^{-1}\operatorname{curl}\mathbf{E} - \operatorname{curl}(\mu_{\mathrm{r}}^{-1}\xi\mathbf{E})] - k^2(\varepsilon_{\mathrm{r}} - \overline{\xi}\mu_{\mathrm{r}}^{-1}\xi)\mathbf{E} = 0, \quad \text{in } \mathbb{R}^3. \tag{4}$$

Denoting by $\mathbf{F}_+$ and $\mathbf{F}_-$ the traces on $\partial\Omega$ from the exterior and interior of Ω, respectively, for a vector function $\mathbf{F}$, we assume transmission conditions across the boundary of Ω. More precisely,

$$\nu \times \mathbf{E}_+ = \nu \times \mathbf{E}_-, \quad \nu \times \operatorname{curl}\mathbf{E}_+ = \nu \times (\mu_{\mathrm{r}}^{-1}\operatorname{curl}\mathbf{E})_- - \nu \times (\mathrm{i}k\mu_{\mathrm{r}}^{-1}\xi\mathbf{E})_-, \quad \text{on } \partial\Omega, \tag{5}$$

where ν is an outward normal vector of Ω. Suppose that the bi-anisotropic medium is illuminated by incident electric and magnetic fields $\mathbf{E}_{\mathrm{in}}$ and $\mathbf{H}_{\mathrm{in}}$, respectively, satisfying

$$\operatorname{curl}\mathbf{H}_{\mathrm{in}} + \mathrm{i}\omega\varepsilon_0\mathbf{E}_{\mathrm{in}} = 0, \qquad \operatorname{curl}\mathbf{E}_{\mathrm{in}} - \mathrm{i}\omega\mu_0\mathbf{H}_{\mathrm{in}} = 0, \quad \text{in } \mathbb{R}^3.$$

We can reformulate (4) in terms of the scattered electric field $\mathbf{u}$, defined by $\mathbf{u} := \mathbf{E} - \mathbf{E}_{\mathrm{in}}$. Since $\operatorname{curl}\operatorname{curl}\mathbf{E}_{\mathrm{in}} - k^2\mathbf{E}_{\mathrm{in}} = 0$, subtracting this equation from (4) we obtain that

$$\begin{aligned}&\operatorname{curl}[\mu_{\mathrm{r}}^{-1}\operatorname{curl}\mathbf{u}] + \mathrm{i}k[\overline{\xi}\mu_{\mathrm{r}}^{-1}\operatorname{curl}\mathbf{u} - \operatorname{curl}(\mu_{\mathrm{r}}^{-1}\xi\mathbf{u})] - k^2(\varepsilon_{\mathrm{r}} - \overline{\xi}\mu_{\mathrm{r}}^{-1}\xi)\mathbf{u}\\ &= \operatorname{curl}[Q\operatorname{curl}\mathbf{E}_{\mathrm{in}}] - \mathrm{i}k[\overline{\xi}\mu_{\mathrm{r}}^{-1}\operatorname{curl}\mathbf{E}_{\mathrm{in}} - \operatorname{curl}(\mu_{\mathrm{r}}^{-1}\xi\mathbf{E}_{\mathrm{in}})] + k^2(P - \overline{\xi}\mu_{\mathrm{r}}^{-1}\xi)\mathbf{E}_{\mathrm{in}} \quad \text{in } \mathbb{R}^3,\end{aligned} \tag{6}$$

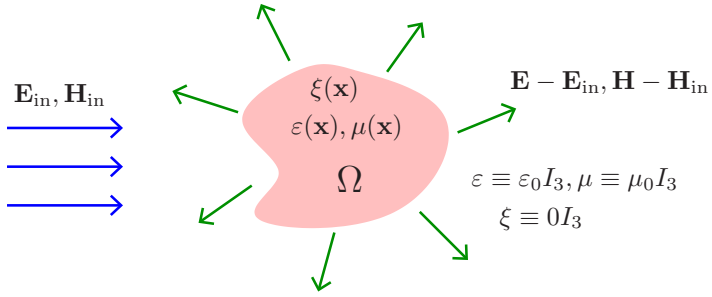

Figure 1. Schematic of the electromagnetic scattering from an inhomogeneous bi-anisotropic medium Ω characterized by matrix-valued functions $\varepsilon(\mathbf{x}), \mu(\mathbf{x}), \xi(\mathbf{x})$.

where the contrasts P and Q are defined by

$$P := \varepsilon_{\rm r} - I_3, \quad Q := I_3 - \mu_{\rm r}^{-1}.$$

Note that we also have corresponding transmission conditions for the scattered field $\mathbf{u}$ following from (5). Furthermore, the scattered field $\mathbf{u}$ must admit the Silver–Müller radiation condition of the form

$$\operatorname{curl} \mathbf{u} \times \frac{\mathbf{x}}{|\mathbf{x}|} - \mathrm{i}k\mathbf{u} = \mathcal{O}(|\mathbf{x}|^{-2}) \quad \text{as } |\mathbf{x}| \longrightarrow \infty, \tag{7}$$

uniformly with respect to $\mathbf{x}$.

We end this section by introducing some basic notations for the paper. Let $\mathcal{O} \subset \mathbb{R}^3$ be a domain (connected and open) with a Lipschitz boundary. We denote

$$\begin{aligned} L^2(\mathcal{O})^3 &= \{\mathbf{v} = (v_1, v_2, v_3)^\top : v_j \in L^2(\mathcal{O}), j = 1, 2, 3\}, \\ H(\operatorname{curl}, \mathcal{O}) &= \{\mathbf{v} \in L^2(\mathcal{O})^3 : \operatorname{curl} \mathbf{v} \in L^2(\mathcal{O})^3\}, \\ H_{\rm loc}(\operatorname{curl}, \mathbb{R}^3) &= \{\mathbf{v} : \mathbb{R}^3 \to \mathbb{C}^3 : \mathbf{v}|_B \in H(\operatorname{curl}, B) \text{ for all balls } B \subset \mathbb{R}^3\}. \end{aligned}$$

Here we indistinctly denote by $(\cdot, \cdot)$ the inner product of $L^2(\mathcal{O})$ or $L^2(\mathcal{O})^3$ and by $\|\cdot\|$ the associated norms, and $H(\operatorname{curl}, \mathcal{O})$ is equipped by the usual inner product

$$(\cdot, \cdot)_{H(\operatorname{curl}, \mathcal{O})} = (\operatorname{curl} \cdot, \operatorname{curl} \cdot) + (\cdot, \cdot).$$

3. Integro-differential formulation and its Fredholm property

In this section we first derive an integro-differential equation for the scattering problem (6) and (7). Second, we show that the integro-differential equation is of the Fredholm type by proving a Gårding inequality for this equation. We need the following important assumption for our analysis.

Assumption 1. *Assume that $\varepsilon_{\rm r}, \mu_{\rm r}, \mu_{\rm r}^{-1}, \xi \in L^\infty(\Omega)^{3\times 3}$ are symmetric almost everywhere and that ξ is real-valued. Furthermore, assume that there exists positive constants c_1, c_2 such that for any $\mathbf{a} \in \mathbb{C}^3$*

$$\operatorname{Re}(\mu_{\rm r}^{-1}\mathbf{a} \cdot \bar{\mathbf{a}}) \geqslant c_1|\mathbf{a}|^2, \quad \operatorname{Re}((\varepsilon_{\rm r} - \xi\mu_{\rm r}^{-1}\xi)\mathbf{a} \cdot \bar{\mathbf{a}}) \geqslant c_2|\mathbf{a}|^2, \quad \||\mu_{\rm r}^{-1}\xi|_2\|_{L^\infty} < c_1c_2.$$

Here $|\cdot|_2$ is the spectral matrix norm. We remark that beside the positivity assumptions we also require that ξ must be 'small' enough, which is common in electromagnetic complex media. Now recall that $P = \varepsilon_r - I_3$, $Q = I_3 - \mu_r^{-1}$. We define the operators $\mathcal{S}$ and $\mathcal{T}$ from $H(\mathrm{curl}\,,\Omega)$ into $L^2(\Omega)^3$ as

$$\mathcal{S}\mathbf{u} := (P - \overline{\xi}\mu_r^{-1}\xi)\mathbf{u} - \frac{\mathrm{i}}{k}\overline{\xi}\mu_r^{-1}\mathrm{curl}\,\mathbf{u}, \quad \mathcal{T}\mathbf{u} := Q\mathrm{curl}\,\mathbf{u} + \mathrm{i}k\mu_r^{-1}\xi\mathbf{u}.$$

Lemma 2. *The operators $\mathcal{S}$ and $\mathcal{T}$ are bounded linear operators from $H(\mathrm{curl}\,,\Omega)$ into $L^2(\Omega)^3$.*

Proof. It is obvious that these are linear operators. We only prove boundedness for $\mathcal{S}$ since the proof is straightforward and similar for $\mathcal{T}$. Indeed, we have

$$\begin{aligned}\|\mathcal{S}\mathbf{u}\| &\leqslant \|(P - \overline{\xi}\mu_r^{-1}\xi)\mathbf{u}\| + \|\frac{\mathrm{i}}{k}\overline{\xi}\mu_r^{-1}\mathrm{curl}\,\mathbf{u}\| \\ &\leqslant \max\{\||P - \overline{\xi}\mu_r^{-1}\xi|_2\|_{L^\infty}, \||\overline{\xi}\mu_r^{-1}|_2\|_{L^\infty}/k\}\|\mathbf{u}\|_{H(\mathrm{curl}\,,\Omega)},\end{aligned}$$

which means that $\mathcal{S}$ is bounded from $H(\mathrm{curl}\,,\Omega)$ into $L^2(\Omega)^3$. □

We can now rewrite (6) as

$$\mathrm{curl}\,\mathrm{curl}\,\mathbf{u} - k^2\mathbf{u} = k^2(\mathcal{S}\mathbf{u} + \mathbf{f}) + \mathrm{curl}\,(\mathcal{T}\mathbf{u} + \mathbf{g}) \quad \text{in } \mathbb{R}^3,$$

where $\mathbf{f} = \mathcal{S}\mathbf{E}_{\mathrm{in}}$ and $\mathbf{g} = \mathcal{T}\mathbf{E}_{\mathrm{in}}$. This equation has a variational formulation as

$$\int_{\mathbb{R}^3}(\mathrm{curl}\,\mathbf{u}\cdot\mathrm{curl}\,\overline{\mathbf{v}} - k^2\mathbf{u}\cdot\overline{\mathbf{v}})\,\mathrm{d}\mathbf{x} = k^2\int_\Omega(\mathcal{S}\mathbf{u} + \mathbf{f})\cdot\overline{\mathbf{v}}\,\mathrm{d}\mathbf{x} + \int_\Omega(\mathcal{T}\mathbf{u} + \mathbf{g})\cdot\mathrm{curl}\,\overline{\mathbf{v}}\,\mathrm{d}\mathbf{x}, \tag{8}$$

for all $\mathbf{v} \in H(\mathrm{curl}\,,\mathbb{R}^3)$ with compact support.

Let Φ be the Green's function to the scattering problem for the scalar Helmholtz equation in $\mathbb{R}^3$

$$\Phi(\mathbf{x},\mathbf{y}) = \frac{\mathrm{e}^{\mathrm{i}k|\mathbf{x}-\mathbf{y}|}}{4\pi|\mathbf{x}-\mathbf{y}|}, \quad \mathbf{x} \neq \mathbf{y}. \tag{9}$$

For $\mathbf{h} \in L^2(\Omega)^3$, the linear operators

$$\begin{aligned}\mathcal{A}\mathbf{h}(\mathbf{x}) &= (k^2 + \nabla\mathrm{div})\int_\Omega \Phi(\mathbf{x},\cdot)\mathbf{h}\,\mathrm{d}\mathbf{y}, \\ \mathcal{B}\mathbf{h}(\mathbf{x}) &= \mathrm{curl}\int_\Omega \Phi(\mathbf{x},\cdot)\mathbf{h}\,\mathrm{d}\mathbf{y},\end{aligned}$$

are bounded from $L^2(\Omega)^3$ into $H_{\mathrm{loc}}(\mathrm{curl}\,,\mathbb{R}^3)$ (see [18]). Using the method of [18] problem (8) can be equivalently formulated as the following integro-differential equation

$$\begin{aligned}\mathbf{u}(\mathbf{x}) = (k^2 + \nabla\mathrm{div})\int_\Omega \Phi(\mathbf{x},\cdot)[(P - \overline{\xi}\mu_r^{-1}\xi)\mathbf{u} - \frac{\mathrm{i}}{k}\overline{\xi}\mu_r^{-1}\mathrm{curl}\,\mathbf{u} + \mathbf{f}]\mathrm{d}\mathbf{y} \\ + \mathrm{curl}\int_\Omega \Phi(\mathbf{x},\cdot)[Q\mathrm{curl}\,\mathbf{u} + \mathrm{i}k\mu_r^{-1}\xi\mathbf{u} + \mathbf{g}]\mathrm{d}\mathbf{y},\end{aligned} \tag{10}$$

or

$$\mathbf{u} - \mathcal{A}\mathcal{S}\mathbf{u} - \mathcal{B}\mathcal{T}\mathbf{u} = \mathcal{A}\mathbf{f} + \mathcal{B}\mathbf{g} \quad \text{in } \mathbb{R}^3. \tag{11}$$

This was proved in [18] for the case of scalar functions ε_r, μ_r and $\xi = 0$. The proof for matrix-valued functions ε_r, μ_r and ξ is actually similar and is therefore omitted here. Next we will prove a Gårding inequality [38] for the operator on the left-hand side of (11), which is also the main result of this section, and is useful for the convergence analysis of our numerical spectral method.

We denote by Φ_0 the exponentially decaying kernel

$$\Phi_0(\mathbf{x}, \mathbf{y}) = \frac{\mathrm{e}^{-k|\mathbf{x}-\mathbf{y}|}}{4\pi|\mathbf{x}-\mathbf{y}|}, \quad \mathbf{x} \neq \mathbf{y}.$$

For $\mathbf{h} \in L^2(\Omega)^3$ we define

$$\mathcal{A}_0\mathbf{h}(\mathbf{x}) = (-k^2 + \nabla\mathrm{div}) \int_\Omega \Phi_0(\mathbf{x}, \cdot)\mathbf{h}\, \mathrm{d}\mathbf{y}, \quad \mathcal{B}_0\mathbf{h}(\mathbf{x}) = \mathrm{curl} \int_\Omega \Phi_0(\mathbf{x}, \cdot)\mathbf{h}\, \mathrm{d}\mathbf{y},$$

which are bounded linear operators from $L^2(\Omega)^3$ into $H(\mathrm{curl}\,, \mathbb{R}^3)$ [18]. The following lemma from [18] is useful to our analysis.

Lemma 3. *For* $\mathbf{h} \in L^2(\Omega)^3$, $\mathcal{A}_0\mathbf{h}$ *and* $\mathcal{B}_0\mathbf{h}$ *uniquely solve*

$$\int_{\mathbb{R}^3} (\mathrm{curl}\, \mathcal{A}_0\mathbf{h} \cdot \mathrm{curl}\, \overline{\mathbf{w}} + k^2 \mathcal{A}_0\mathbf{h} \cdot \overline{\mathbf{w}})\, \mathrm{d}\mathbf{x} = -k^2 \int_\Omega \mathbf{h} \cdot \overline{\mathbf{w}}\, \mathrm{d}\mathbf{x},$$
$$\int_{\mathbb{R}^3} (\mathrm{curl}\, \mathcal{B}_0\mathbf{h} \cdot \mathrm{curl}\, \overline{\mathbf{w}} + k^2 \mathcal{B}_0\mathbf{h} \cdot \overline{\mathbf{w}})\, \mathrm{d}\mathbf{x} = \int_\Omega \mathbf{h} \cdot \mathrm{curl}\, \overline{\mathbf{w}}\, \mathrm{d}\mathbf{x},$$

for all $\mathbf{w} \in H(\mathrm{curl}\,, \mathbb{R}^3)$.

Let B_ρ be a ball with the center at the origin and radius ρ, and suppose that $\overline{\Omega} \subset B_\rho$. We need the following inner product in our analysis

$$(\cdot, \cdot)_{k,H(\mathrm{curl}\,,B_\rho)} = (\mathrm{curl}\, \cdot, \mathrm{curl}\, \cdot) + k^2(\cdot, \cdot). \tag{12}$$

Now let $\mathbf{h}_n$ be smooth functions with compact support in Ω such that $\mathbf{h}_n \to \mathbf{h}$ in $L^2(\Omega)^3$. Then we have from lemma 3 that $\mathrm{curl}\,\mathrm{curl}\, \mathcal{A}_0\mathbf{h}_n + k^2\mathcal{A}_0\mathbf{h}_n = -k^2\mathbf{h}_n$ in $L^2(\mathbb{R}^3)^3$. Multiplying both sides of this equation by $\mathbf{v} \in H(\mathrm{curl}\,, B_\rho)$, using Green's theorem and taking the limit $n \to \infty$ we have

$$(\mathcal{A}_0\mathbf{h}, \mathbf{v})_{k,H(\mathrm{curl}\,,B_\rho)} = -k^2(\mathbf{h}, \mathbf{v}) - \int_{\partial B_\rho} (\nu \times \mathrm{curl}\, \mathcal{A}_0\mathbf{h}) \cdot (\nu \times \overline{\mathbf{v}}) \times \nu\, \mathrm{d}s, \tag{13}$$

where ν is the outward normal vector of B_ρ. Similarly for $\mathcal{B}_0$ we also have

$$(\mathcal{B}_0\mathbf{h}, \mathbf{v})_{k,H(\mathrm{curl}\,,B_\rho)} = (\mathbf{h}, \mathrm{curl}\, \mathbf{v}) - \int_{\partial B_\rho} (\nu \times \mathrm{curl}\, \mathcal{B}_0\mathbf{h}) \cdot (\nu \times \overline{\mathbf{v}}) \times \nu\, \mathrm{d}s. \tag{14}$$

We notice that for $\mathbf{y} \in \Omega$, $\Phi_0(\cdot, \mathbf{y})$ is smooth on ∂B_ρ. Therefore, the kernel of $\mathcal{A}_0$ and $\mathcal{B}_0$ is smooth on ∂B_ρ, and the traces on ∂B_ρ in the variational equations above are well defined.

Now we are ready to prove the Gårding inequality.

Theorem 4. *Suppose that assumption 1 holds true. Then there exists a positive constant* C *and a compact operator* K *on* $H(\mathrm{curl}\,, B_\rho)$ *such that*

$$\mathrm{Re}\,(\mathbf{u} - \mathcal{A}\mathcal{S}\mathbf{u} - \mathcal{B}\mathcal{T}\mathbf{u}, \mathbf{u})_{k,H(\mathrm{curl}\,,B_\rho)} \geqslant C\|\mathbf{u}\|^2_{k,H(\mathrm{curl}\,,B_\rho)} - \mathrm{Re}\,(K\mathbf{u}, \mathbf{u})_{k,H(\mathrm{curl}\,,B_\rho)}, \tag{15}$$

for all $\mathbf{u} \in H(\mathrm{curl}\,, B_\rho)$.

Proof. Applying (13) and (14) for $\mathbf{h} = \mathcal{S}\mathbf{u}$ and $\mathbf{h} = \mathcal{T}\mathbf{u}$, respectively, choosing $\mathbf{v} = \mathbf{u}$ and adding the two resulting equations up we obtain

$$\begin{aligned}
&(\mathcal{A}_0\mathcal{S}\mathbf{u} + \mathcal{B}_0\mathcal{T}\mathbf{u}, \mathbf{u})_{k,H(\mathrm{curl}\,,B_\rho)} \\
&= -\int_{\partial B_\rho} (\nu \times \mathrm{curl}\,(\mathcal{A}_0\mathcal{S}\mathbf{u} + \mathcal{B}_0\mathcal{T}\mathbf{u})) \cdot (\nu \times \overline{\mathbf{u}}) \times \nu \,\mathrm{d}s \\
&\quad - k^2 \int_\Omega ((P - \overline{\xi}\mu_{\mathrm{r}}^{-1}\xi)\mathbf{u} - \frac{\mathrm{i}}{k}\overline{\xi}\mu_{\mathrm{r}}^{-1}\mathrm{curl}\,\mathbf{u}) \cdot \overline{\mathbf{u}}\,\mathrm{d}\mathbf{x} + \int_\Omega (Q\mathrm{curl}\,\mathbf{u} + \mathrm{i}k\mu_{\mathrm{r}}^{-1}\xi\mathbf{u}) \cdot \mathrm{curl}\,\overline{\mathbf{u}}\,\mathrm{d}\mathbf{x}.
\end{aligned}$$

The smoothness of the kernel Φ_0 on ∂B_ρ allows us to obtain the compactness of the operator $K_1 : H(\mathrm{curl}\,, B_\rho) \to H(\mathrm{curl}\,, B_\rho)$ defined by

$$(K_1\mathbf{u}, \mathbf{u})_{k,H(\mathrm{curl}\,,B_\rho)} = \int_{\partial B_\rho} (\nu \times \mathrm{curl}\,(A_0\mathcal{S}\mathbf{u} + \mathcal{B}_0\mathcal{T}\mathbf{u})) \cdot (\nu \times \overline{\mathbf{u}}) \times \nu \,\mathrm{d}s.$$

Straightforward calculations lead to

$$\begin{aligned}
(\mathbf{u} - \mathcal{A}_0\mathcal{S}\mathbf{u} - \mathcal{B}_0\mathcal{T}\mathbf{u} - K_1\mathbf{u}, \mathbf{u})_{k,H(\mathrm{curl}\,,B_\rho)} &= \int_{B_\rho} \mu_{\mathrm{r}}^{-1}\mathrm{curl}\,\mathbf{u} \cdot \mathrm{curl}\,\overline{\mathbf{u}} + k^2(\varepsilon_r - \overline{\xi}\mu_{\mathrm{r}}^{-1}\xi)\mathbf{u} \cdot \overline{\mathbf{u}}\mathrm{d}\mathbf{x} \\
&\quad - \int_{B_\rho} \mathrm{i}k(\mu_{\mathrm{r}}^{-1}\xi\mathbf{u} \cdot \mathrm{curl}\,\overline{\mathbf{u}} + \overline{\xi}\mu_{\mathrm{r}}^{-1}\mathrm{curl}\,\mathbf{u} \cdot \overline{\mathbf{u}})\mathrm{d}\mathbf{x}.
\end{aligned}$$

Taking the real part of this equation and using assumption 1 we obtain

$$\begin{aligned}
\mathrm{Re}\,(\mathbf{u} - \mathcal{A}_0\mathcal{S}\mathbf{u} - \mathcal{B}_0\mathcal{T}\mathbf{u} - K_1\mathbf{u}, \mathbf{u})_{k,H(\mathrm{curl}\,,B_\rho)} &\geqslant \int_{B_\rho} c_1|\mathrm{curl}\,\mathbf{u}|^2 + k^2c_2|\mathbf{u}|^2\mathrm{d}\mathbf{x} \\
&\quad + k\mathrm{Im}\int_{B_\rho} (\mu_{\mathrm{r}}^{-1}\xi\mathbf{u} \cdot \mathrm{curl}\,\overline{\mathbf{u}} + \overline{\xi}\mu_{\mathrm{r}}^{-1}\mathrm{curl}\,\mathbf{u} \cdot \overline{\mathbf{u}})\mathrm{d}\mathbf{x}.
\end{aligned} \tag{16}$$

Since we assume that ξ is real-valued and that ξ and μ_{r} are symmetric, we have

$$\overline{\xi}\mu_{\mathrm{r}}^{-1}\mathrm{curl}\,\mathbf{u} \cdot \overline{\mathbf{u}} = \mu_{\mathrm{r}}^{-1}\xi\,\overline{\mathbf{u}} \cdot \mathrm{curl}\,\mathbf{u}.$$

We also have that

$$\begin{aligned}
\frac{c_1}{2}|\mathrm{curl}\,\mathbf{u}|^2 + k\mathrm{Im}\,(\mu_{\mathrm{r}}^{-1}\xi\mathbf{u} \cdot \mathrm{curl}\,\overline{\mathbf{u}}) + \frac{k^2}{2c_1}|\mu_{\mathrm{r}}^{-1}\xi\mathbf{u}|^2 &= \left|\sqrt{\frac{c_1}{2}}\mathrm{curl}\,\mathbf{u} - \frac{\mathrm{i}k}{\sqrt{2c_1}}\mu_{\mathrm{r}}^{-1}\xi\mathbf{u}\right|^2 \\
\frac{c_1}{2}|\mathrm{curl}\,\mathbf{u}|^2 + k\mathrm{Im}\,(\mu_{\mathrm{r}}^{-1}\xi\overline{\mathbf{u}} \cdot \mathrm{curl}\,\mathbf{u}) + \frac{k^2}{2c_1}|\mu_{\mathrm{r}}^{-1}\xi\overline{\mathbf{u}}|^2 &= \left|\sqrt{\frac{c_1}{2}}\mathrm{curl}\,\mathbf{u} - \frac{\mathrm{i}k}{\sqrt{2c_1}}\mu_{\mathrm{r}}^{-1}\xi\overline{\mathbf{u}}\right|^2.
\end{aligned}$$

Using these equations in (16) leads to

$$\begin{aligned}\mathrm{Re}\,(\mathbf{u}-\mathcal{A}_0\mathcal{S}\mathbf{u}-\mathcal{B}_0\mathcal{T}\mathbf{u}-K_1\mathbf{u},\mathbf{u})_{k,H(\mathrm{curl},B_\rho)} \geqslant & \left\|\sqrt{\frac{c_1}{2}}\mathrm{curl}\,\mathbf{u}-\frac{\mathrm{i}k}{\sqrt{2c_1}}\mu_{\mathrm{r}}^{-1}\xi\mathbf{u}\right\|^2\\ &+\left\|\sqrt{\frac{c_1}{2}}\mathrm{curl}\,\mathbf{u}-\frac{\mathrm{i}k}{\sqrt{2c_1}}\mu_{\mathrm{r}}^{-1}\xi\overline{\mathbf{u}}\right\|^2\\ &+k^2\left(c_2\|\mathbf{u}\|^2-\frac{1}{2c_1}\|\mu_{\mathrm{r}}^{-1}\xi\mathbf{u}\|^2-\frac{1}{2c_1}\|\mu_{\mathrm{r}}^{-1}\xi\overline{\mathbf{u}}\|^2\right).\end{aligned} \tag{17}$$

We can estimate the last term as

$$c_2\|\mathbf{u}\|^2-\frac{1}{2c_1}\|\mu_{\mathrm{r}}^{-1}\xi\mathbf{u}\|^2-\frac{1}{2c_1}\|\mu_{\mathrm{r}}^{-1}\xi\overline{\mathbf{u}}\|^2 \geqslant \left(c_2-\frac{1}{c_1}\||\mu_{\mathrm{r}}^{-1}\xi|_2\|_{L^\infty}\right)\|\mathbf{u}\|^2. \tag{18}$$

For the convenience of the presentation we set

$$\gamma = c_2-\frac{1}{c_1}\||\mu_{\mathrm{r}}^{-1}\xi|_2\|_{L^\infty} > 0.$$

Now we estimate

$$\begin{aligned}&k^2\|\mathbf{u}\|^2+\left\|\sqrt{\frac{c_1}{2}}\mathrm{curl}\,\mathbf{u}\right\|^2 \leqslant \left(k\|\mathbf{u}\|+\left\|\sqrt{\frac{c_1}{2}}\mathrm{curl}\,\mathbf{u}\right\|\right)^2\\ &\leqslant \left(k\|\mathbf{u}\|+\left\|\sqrt{\frac{c_1}{2}}\mathrm{curl}\,\mathbf{u}-\frac{\mathrm{i}k}{\sqrt{2c_1}}\mu_{\mathrm{r}}^{-1}\xi\mathbf{u}\right\|+\left\|\frac{\mathrm{i}k}{\sqrt{2c_1}}\mu_{\mathrm{r}}^{-1}\xi\mathbf{u}\right\|\right)^2\\ &\leqslant 2\left(\left\|\sqrt{\frac{c_1}{2}}\mathrm{curl}\,\mathbf{u}-\frac{\mathrm{i}k}{\sqrt{2c_1}}\mu_{\mathrm{r}}^{-1}\xi\mathbf{u}\right\|^2+k^2\left(1+\frac{\||\mu_{\mathrm{r}}^{-1}\xi|_2\|_{L^\infty}}{\sqrt{2c_1}}\right)^2\|\mathbf{u}\|^2\right)\\ &\leqslant 2\max\left\{1,\left(\frac{\sqrt{2c_1}+\||\mu_{\mathrm{r}}^{-1}\xi|_2\|_{L^\infty}}{\sqrt{2c_1}\sqrt{\gamma}}\right)^2\right\}\left(\left\|\sqrt{\frac{c_1}{2}}\mathrm{curl}\,\mathbf{u}-\frac{\mathrm{i}k}{\sqrt{2c_1}}\mu_{\mathrm{r}}^{-1}\xi\mathbf{u}\right\|^2+k^2\gamma\|\mathbf{u}\|^2\right).\end{aligned}$$

Therefore, we have shown that there exists a constant

$$C=\frac{\min\left\{1,\frac{c_1}{2}\right\}}{2\max\left\{1,\left(\frac{\sqrt{2c_1}+\||\mu_{\mathrm{r}}^{-1}\xi|_2\|_{L^\infty}}{\sqrt{2c_1}\sqrt{\gamma}}\right)^2\right\}},$$

such that

$$\left\|\sqrt{\frac{c_1}{2}}\mathrm{curl}\,\mathbf{u}-\frac{\mathrm{i}k}{\sqrt{2c_1}}\mu_{\mathrm{r}}^{-1}\xi\mathbf{u}\right\|^2+k^2\gamma\|\mathbf{u}\|^2 \geqslant C\|\mathbf{u}\|^2_{k,H(\mathrm{curl},B_\rho)}. \tag{19}$$

From (17)–(19) we obtain that

$$\mathrm{Re}\,(\mathbf{u}-\mathcal{A}_0\mathcal{S}\mathbf{u}-\mathcal{B}_0\mathcal{T}\mathbf{u}-K_1\mathbf{u},\mathbf{u})_{k,H(\mathrm{curl},B_\rho)} \geqslant C\|\mathbf{u}\|^2_{k,H(\mathrm{curl},B_\rho)}.$$

Therefore

$$\begin{aligned}\mathrm{Re}\,(\mathbf{u}-\mathcal{A}\mathcal{S}\mathbf{u}-\mathcal{B}\mathcal{T}\mathbf{u},\mathbf{u})_{k,H(\mathrm{curl},B_\rho)} \geqslant & C\|\mathbf{u}\|^2_{k,H(\mathrm{curl},B_\rho)}+\mathrm{Re}\,(K_1\mathbf{u},\mathbf{u})_{k,H(\mathrm{curl},B_\rho)}\\ &+\mathrm{Re}\,((\mathcal{A}-\mathcal{A}_0)\mathcal{S}\mathbf{u}+(\mathcal{B}-\mathcal{B}_0)\mathcal{T}\mathbf{u},\mathbf{u})_{k,H(\mathrm{curl},B_\rho)}.\end{aligned}$$

It is known from [18] that the operators $\mathcal{A}-\mathcal{A}_0, \mathcal{B}-B_0$ can be written as integral operators with weakly singular kernels. Therefore, the operator K_2 defined by

$$(K_2\mathbf{u},\mathbf{u})_{k,H(\mathrm{curl},B_\rho)} = ((\mathcal{A}-\mathcal{A}_0)\mathcal{S}\mathbf{u} + (\mathcal{B}-\mathcal{B}_0)\mathcal{T}\mathbf{u},\mathbf{u})_{k,H(\mathrm{curl},B_\rho)},$$

is compact on $H(\mathrm{curl}\,,B_\rho)$. Setting $K := K_1 + K_2$, we obtain the desired Gårding inequality. □

The following corollary follows immediately from theorem 8.

Corollary 5. *The direct problem or the integro-differential equation (10) is uniquely solvable if and only if the corresponding homogeneous problem only has a trivial solution.*

4. Uniqueness of solution

Thanks to corollary 5 we only have to prove the uniqueness of the solution, which is the main goal of this section. To do so we need the assumption on the absorbing material parameters. More precisely, we assume for all $\mathbf{a}\in\mathbb{C}^3$ that

$$\mathrm{Im}\,(\varepsilon_\mathrm{r}\mathbf{a}\cdot\overline{\mathbf{a}}) \geqslant \beta|\mathbf{a}|^2, \quad \mathrm{Im}\,(\mu_\mathrm{r}^{-1}\mathbf{a}\cdot\overline{\mathbf{a}}) \leqslant -\alpha|\mathbf{a}|^2, \tag{20}$$

where α and β are positive constants such that

$$\||\mu_\mathrm{r}^{-1}|_2\|_{L^\infty}^2 < \alpha^2 + \alpha\beta\||\xi|_2\|_{L^\infty}^{-2}.$$

We remark that the latter inequality constraint is quite reasonable since the norm $\||\xi|_2\|_{L^\infty}^{-2}$ is supposed to be large following assumption 1.

Theorem 6. *If assumption 1 and (20) hold true, then solution* $\mathbf{u}$ *to the variational problem (8) for* $\mathbf{f}=\mathbf{g}=0$ *must vanish in* $\mathbb{R}^3$.

Proof. Assume that $\mathbf{u}$ is a solution to problem (8) for $\mathbf{f}=\mathbf{g}=0$. Recall that $\overline{\Omega}\subset B_\rho$. Let $\phi\in C_0^\infty(\mathbb{R}^3)$ be a cut-off function satisfying $\phi=1$ in $\overline{B_\rho}$ and $\phi=0$ for $|\mathbf{x}|\geqslant 2\rho$. Choosing $\mathbf{v}=\phi\mathbf{u}$ in (8) leads to

$$\begin{aligned}
&\int_{B_\rho}(\mu_\mathrm{r}^{-1}\mathrm{curl}\,\mathbf{u}\cdot\mathrm{curl}\,\overline{\mathbf{u}} + \mathrm{i}k\xi\mu_\mathrm{r}^{-1}\mathrm{curl}\,\mathbf{u}\cdot\overline{\mathbf{u}} - \mathrm{i}k\mu_\mathrm{r}^{-1}\xi\mathbf{u}\cdot\mathrm{curl}\,\overline{\mathbf{u}} - k^2(\varepsilon_\mathrm{r}-\xi\mu_\mathrm{r}^{-1}\xi)\mathbf{u}\cdot\overline{\mathbf{u}})\,\mathrm{d}\mathbf{x}\\
&= -\int_{\rho<|\mathbf{x}|<2\rho}(\mathrm{curl}\,\mathbf{u}\cdot\mathrm{curl}\,(\phi\overline{\mathbf{u}}) - k^2\mathbf{u}\cdot\phi\overline{\mathbf{u}})\mathrm{d}\mathbf{x}\\
&= \int_{|\mathbf{x}|=\rho}(\mathrm{curl}\,\mathbf{u}\times\nu)\cdot\overline{\mathbf{u}}\,\mathrm{d}s.
\end{aligned}$$

We recall that ξ is assumed to be real-valued and that $\mu_\mathrm{r}, \varepsilon_\mathrm{r}, \xi$ are symmetric. Therefore we can rewrite the left-hand side of this equation as

$$\begin{aligned}
&\int_{B_\rho}(\mu_\mathrm{r}^{-1}\mathrm{curl}\,\mathbf{u}\cdot\mathrm{curl}\,\overline{\mathbf{u}} + \mathrm{i}k\mu_\mathrm{r}^{-1}\xi\overline{\mathbf{u}}\cdot\mathrm{curl}\,\mathbf{u} - \mathrm{i}k\mu_\mathrm{r}^{-1}\xi\mathbf{u}\cdot\mathrm{curl}\,\overline{\mathbf{u}} + k^2\mu_\mathrm{r}^{-1}\xi\mathbf{u}\cdot\xi\overline{\mathbf{u}} - k^2\varepsilon_\mathrm{r}\mathbf{u}\cdot\overline{\mathbf{u}})\mathrm{d}\mathbf{x}\\
&\qquad = \int_{|\mathbf{x}|=\rho}(\mathrm{curl}\,\mathbf{u}\times\nu)\cdot\overline{\mathbf{u}}\,\mathrm{d}s.
\end{aligned} \tag{21}$$

Taking the imaginary part of (21) implies that

$$\begin{aligned}\operatorname{Im}\int_{|\mathbf{x}|=\rho}(\operatorname{curl}\mathbf{u}\times\nu)\cdot\overline{\mathbf{u}}\,\mathrm{d}s &\leqslant -\alpha\|\operatorname{curl}\mathbf{u}\|^2-\alpha\|k\xi\mathbf{u}\|^2-\beta\|k\mathbf{u}\|^2\\ &\quad +k\int_{B_\rho}\operatorname{Re}\,(\mu_{\mathrm{r}}^{-1}\operatorname{curl}\mathbf{u}\cdot\xi\overline{\mathbf{u}})\mathrm{d}\mathbf{x}-k\int_{B_\rho}\operatorname{Re}\,(\mu_{\mathrm{r}}^{-1}\operatorname{curl}\overline{\mathbf{u}}\cdot\xi\mathbf{u})\mathrm{d}\mathbf{x}.\end{aligned}\tag{22}$$

For any $\eta>0$ we have

$$\begin{aligned}k\int_{B_\rho}\operatorname{Re}\,(\mu_{\mathrm{r}}^{-1}\operatorname{curl}\mathbf{u}\cdot\xi\overline{\mathbf{u}})\mathrm{d}\mathbf{x}&=\frac{1}{2\alpha\eta}\|k\xi\mathbf{u}\|^2+\frac{\eta\alpha}{2}\|\mu_{\mathrm{r}}^{-1}\operatorname{curl}\mathbf{u}\|^2\\ &\quad-\left\|\frac{1}{\sqrt{2\alpha\eta}}k\xi\overline{\mathbf{u}}-\sqrt{\frac{\eta\alpha}{2}}\mu_{\mathrm{r}}^{-1}\operatorname{curl}\mathbf{u}\right\|^2,\\ -k\int_{B_\rho}\operatorname{Re}\,(\mu_{\mathrm{r}}^{-1}\operatorname{curl}\overline{\mathbf{u}}\cdot\xi\mathbf{u})\mathrm{d}\mathbf{x}&=\frac{1}{2\alpha\eta}\|k\xi\mathbf{u}\|^2+\frac{\eta\alpha}{2}\|\mu_{\mathrm{r}}^{-1}\operatorname{curl}\overline{\mathbf{u}}\|^2\\ &\quad-\left\|\frac{1}{\sqrt{2\alpha\eta}}k\xi\mathbf{u}+\sqrt{\frac{\eta\alpha}{2}}\mu_{\mathrm{r}}^{-1}\operatorname{curl}\overline{\mathbf{u}}\right\|^2.\end{aligned}$$

Substituting these equalities in (22) and using $\|\mu_{\mathrm{r}}^{-1}\operatorname{curl}\mathbf{u}\|^2\leqslant\||\mu_{\mathrm{r}}^{-1}|_2\|_{L^\infty}^2\|\operatorname{curl}\mathbf{u}\|^2$ and $-\beta\|k\mathbf{u}\|^2\leqslant-\beta\||\xi|_2\|_{L^\infty}^{-2}\|k\xi\mathbf{u}\|^2$ we obtain

$$\begin{aligned}&\operatorname{Im}\int_{|\mathbf{x}|=\rho}(\operatorname{curl}\mathbf{u}\times\nu)\cdot\overline{\mathbf{u}}\,\mathrm{d}\mathbf{x}\\ &\leqslant\left(\||\mu_{\mathrm{r}}^{-1}|_2\|_{L^\infty}^2\eta\alpha-\alpha\right)\|\operatorname{curl}\mathbf{u}\|^2+\left(\frac{1}{\eta\alpha}-\alpha-\beta\||\xi|_2\|_{L^\infty}^{-2}\right)\|k\xi\mathbf{u}\|^2\\ &-\left\|\frac{1}{\sqrt{2\alpha\eta}}k\xi\overline{\mathbf{u}}-\sqrt{\frac{\eta\alpha}{2}}\mu_{\mathrm{r}}^{-1}\operatorname{curl}\mathbf{u}\right\|^2-\left\|\frac{1}{\sqrt{2\alpha\eta}}k\xi\mathbf{u}+\sqrt{\frac{\eta\alpha}{2}}\mu_{\mathrm{r}}^{-1}\operatorname{curl}\overline{\mathbf{u}}\right\|^2.\end{aligned}\tag{23}$$

Using assumption (20) we can choose η such that

$$\frac{1}{\alpha^2+\alpha\beta\||\xi|_2\|_{L^\infty}^{-2}}<\eta<\frac{1}{\||\mu_{\mathrm{r}}^{-1}|_2\|_{L^\infty}^2},$$

which implies that the first two terms on the right-hand side of (23) are nonpositive. Therefore, we obtain the estimate

$$\operatorname{Im}\int_{|\mathbf{x}|=\rho}(\operatorname{curl}\mathbf{u}\times\nu)\cdot\overline{\mathbf{u}}\,\mathrm{d}\mathbf{x}\leqslant 0.$$

Using this estimate we have

$$\begin{aligned}\int_{|\mathbf{x}|=\rho}\left|\operatorname{curl}\mathbf{u}\times\frac{\mathbf{x}}{|\mathbf{x}|}-\mathrm{i}k\mathbf{u}\right|^2\mathrm{d}s&=\int_{|\mathbf{x}|=\rho}(|\operatorname{curl}\mathbf{u}|^2+k^2|\mathbf{u}|^2)\mathrm{d}s-2k\operatorname{Im}\int_{|\mathbf{x}|=\rho}(\operatorname{curl}\mathbf{u}\times\nu)\cdot\overline{\mathbf{u}}\,\mathrm{d}\mathbf{x}\\ &\geqslant\int_{|\mathbf{x}|=\rho}(|\operatorname{curl}\mathbf{u}|^2+k^2|\mathbf{u}|^2)\mathrm{d}s.\end{aligned}$$

Letting $\rho\to\infty$ and using the radiation condition we obtain

$$\lim_{\rho\to\infty}\int_{|\mathbf{x}|=\rho}|\mathbf{u}|^2\mathrm{d}s=\lim_{\rho\to\infty}\int_{|\mathbf{x}|=\rho}|\mathrm{curl}\,\mathbf{u}|^2\mathrm{d}s=0.$$

Recall that we have $\mathrm{curl}\,\mathrm{curl}\,\mathbf{u}-k^2\mathbf{u}=0$ in $\mathbb{R}^3\setminus\overline{B_\rho}$, which implies that $\Delta\mathbf{u}+k^2\mathbf{u}=0$ in $\mathbb{R}^3\setminus\overline{B_\rho}$. Therefore, using Rellich's lemma (see [12, lemma 2.12]) and the analytic continuation one can deduce that $\mathbf{u}=0$ in $\mathbb{R}^3\setminus\overline{\Omega}$. This result also implies $\mathrm{Im}\int_{|\mathbf{x}|=\rho}(\mathrm{curl}\,\mathbf{u}\times\nu)\cdot\overline{\mathbf{u}}\,\mathrm{d}\mathbf{x}=0$ which allows us to obtain the following from (23)

$$\xi\mathbf{u}=\mathrm{curl}\,\mathbf{u}=0,\quad\text{in }\Omega.$$

The latter and (21) implies that $\mathbf{u}=0$ in Ω since $\varepsilon_\mathrm{r}-\xi\mu_\mathrm{r}^{-1}\xi$ is positive definite by assumption 1. Therefore, we have shown the solution $\mathbf{u}=0$ in $H(\mathrm{curl}\,,\mathbb{R}^3)$, which completes the proof. □

5. Fast numerical solution to the direct problem

Solving the direct problem is equivalent to solving the integro-differential equation

$$\mathbf{u}-\mathcal{A}\mathcal{S}\mathbf{u}-\mathcal{B}\mathcal{T}\mathbf{u}=\mathcal{A}\mathbf{f}+\mathcal{B}\mathbf{g}\quad\text{in }H_{\mathrm{loc}}(\mathrm{curl}\,,\mathbb{R}^3).\tag{24}$$

We will develop a fast spectral Galerkin method to solve (24). This spectral method exploits the convolution structure of the integro-differential operators, which enables the use of FFT in the numerical implementation. To this end we first need to establish a suitable periodization of (24).

Recall that $\overline{\Omega}\subset B_\rho$. For $R>2\rho$, we consider the cube

$$\Omega_R=\{\mathbf{x}\in\mathbb{R}^3:|x_j|<R,j=1,2,3\},$$

and define the new (smoothed) kernel $\mathcal{K}$ in Ω_R as follows

$$\mathcal{K}(\mathbf{x})=\begin{cases}\psi(\mathbf{x})\Phi(\mathbf{x}), & \mathbf{x}\in B_R\\ 0, & \mathbf{x}\in\Omega_R\setminus\overline{B_R},\end{cases}\tag{25}$$

where $\psi\in C_0^\infty(B_R)$ such that $\psi(\mathbf{x})=1$ in $B_{2\rho}$.

After that we extend $\mathcal{K},P,Q,\xi,\mathbf{f}$ and $\mathbf{g}$ from Ω_R to $\mathbb{R}^3$ as $2R$-periodic functions with respect to all variables. The orthonormal basis of $L^2(\Omega_R)$ and Fourier coefficients of $\mathbf{f}\in L^2(\Omega_R)$ are given by

$$\phi_\mathbf{j}(\mathbf{x})=\frac{1}{\sqrt{8R^3}}\exp\left(\mathrm{i}\pi\mathbf{j}\cdot\frac{\mathbf{x}}{R}\right),\quad\widehat{\mathbf{f}}(\mathbf{j})=\int_{\Omega_R}\mathbf{f}\,\overline{\phi_\mathbf{j}}\,\mathrm{d}\mathbf{x},\quad\mathbf{j}\in\mathbb{Z}^3.\tag{26}$$

For a periodization of (24) we define $H_\mathrm{p}(\mathrm{curl}\,,\Omega_R)$ as a subspace in $L^2(\Omega_R)^3$ containing functions $\mathbf{f}$ such that

$$\|\mathbf{f}\|^2_{H_\mathrm{p}(\mathrm{curl}\,,\Omega_R)}=\sum_{\mathbf{j}\in\mathbb{Z}^3}\left(k^2|\widehat{\mathbf{f}}(\mathbf{j})|^2+|(\mathbf{j}\pi/R)\times\widehat{\mathbf{f}}(\mathbf{j})|^2\right)<\infty.\tag{27}$$

Note that a function $\mathbf{f}\in H_\mathrm{p}(\mathrm{curl}\,,\Omega_R)$ is $2R$-periodic in x_1,x_2 and x_3, and that the norm $\|\mathbf{f}\|_{H_\mathrm{p}(\mathrm{curl}\,,\Omega_R)}$ on $H_\mathrm{p}(\mathrm{curl}\,,\Omega_R)$ is equivalent to the usual norm $\|\mathbf{f}\|_{k,H(\mathrm{curl}\,,\Omega_R)}$.

We define periodic integro-differential operators $\mathcal{A}_\mathrm{p}$, $\mathcal{B}_\mathrm{p}$ from $L^2(\Omega_R)^3$ into $H_\mathrm{p}(\mathrm{curl}\,,\Omega_R)$ by

$$\mathcal{A}_{\mathrm{p}}\mathbf{f}(\mathbf{x}) = (k^2 + \nabla\mathrm{div}) \int_{\Omega_R} \mathcal{K}(\mathbf{x}, \cdot)\mathbf{f}\, \mathrm{d}\mathbf{y}, \quad \mathcal{B}_{\mathrm{p}}\mathbf{f}(\mathbf{x}) = \mathrm{curl} \int_{\Omega_R} \mathcal{K}(\mathbf{x}, \cdot)\mathbf{f}\, \mathrm{d}\mathbf{y} \quad \text{in } \Omega_R.$$

These operators are continuous linear operators, see [30]. Let us now consider the periodic version of the original integro-differential equation (24)

$$\mathbf{u} - \mathcal{A}_{\mathrm{p}}\mathcal{S}\mathbf{u} - \mathcal{B}_{\mathrm{p}}\mathcal{T}\mathbf{u} = \mathcal{A}_{\mathrm{p}}\mathbf{f} + \mathcal{B}_{\mathrm{p}}\mathbf{g} \quad \text{in } H_{\mathrm{p}}(\mathrm{curl}\,, \Omega_R). \tag{28}$$

The next theorem shows that solving the original integro-differential equation (24) is now equivalent to solving the periodic integro-differential equation (28).

Theorem 7. *Suppose that assumption 1 and (20) hold true. The periodic integro-differential equation (28) has a unique solution* $\mathbf{v} \in H_{\mathrm{p}}(\mathrm{curl}\,, \Omega_R)$ *for all* $\mathbf{f}, \mathbf{g} \in L^2(\Omega)^3$. *Furthermore,* $\mathbf{v}|_{B_\rho} \in H(\mathrm{curl}\,, B_\rho)$ *solves the original integro-differential equation (24).*

Proof. Let $\mathbf{f}, \mathbf{g} \in L^2(\Omega)^3$ and we extend them by zero outside of Ω. It is proved in the previous sections that the integro-differential equation (24) is uniquely solvable. Let $\mathbf{u} \in H(\mathrm{curl}\,, B_\rho)$ be this unique solution. We define $\mathbf{v}$ by

$$\mathbf{v} = \mathcal{A}_{\mathrm{p}}(\mathcal{S}\mathbf{u} + \mathbf{f}) + \mathcal{B}_{\mathrm{p}}(\mathcal{T}\mathbf{u} + \mathbf{g}). \tag{29}$$

Then $\mathbf{v}$ belongs to $H_{\mathrm{p}}(\mathrm{curl}\,, \Omega_R)$ thanks to the fact that $\mathcal{S}\mathbf{u} + \mathbf{f}$ and $\mathcal{T}\mathbf{u} + \mathbf{g}$ are in $L^2(\Omega)^3$, and that $\mathcal{A}_{\mathrm{p}}, \mathcal{B}_{\mathrm{p}}$ are bounded linear operators from $L^2(\Omega)^3$ to $H_{\mathrm{p}}(\mathrm{curl}\,, \Omega_R)$. Now we show that $\mathbf{v}|_{B_\rho} = \mathbf{u}$. Recall that for $|\mathbf{x} - \mathbf{y}| < 2\rho$, we know from (25) that $\mathcal{K}(\mathbf{x}, \mathbf{y}) = \Phi(\mathbf{x}, \mathbf{y})$. Therefore, for $\mathbf{x} \in B_\rho$ and $\mathbf{y} \in \Omega \subset B_\rho$, we have

$$\begin{aligned}
\mathcal{A}_{\mathrm{p}}(\mathcal{S}\mathbf{u} + \mathbf{f})(\mathbf{x}) &= (k^2 + \nabla\mathrm{div}) \int_{\Omega_R} \mathcal{K}(\mathbf{x}, \cdot)(\mathcal{S}\mathbf{u} + \mathbf{f})\, \mathrm{d}\mathbf{y} \\
&= (k^2 + \nabla\mathrm{div}) \int_{\Omega} \Phi(\mathbf{x}, \cdot)(\mathcal{S}\mathbf{u} + \mathbf{f})\, \mathrm{d}\mathbf{y} \\
&= \mathcal{A}(\mathcal{S}\mathbf{u} + \mathbf{f})(\mathbf{x}).
\end{aligned}$$

Similarly we obtain $\mathcal{B}_{\mathrm{p}}(\mathcal{T}\mathbf{u} + \mathbf{g})(\mathbf{x}) = \mathcal{B}(\mathcal{T}\mathbf{u} + \mathbf{g})(\mathbf{x})$ for $\mathbf{x} \in B_\rho$. Therefore, we have that for $\mathbf{x} \in B_\rho$

$$\mathbf{v}(\mathbf{x}) = \mathcal{A}_{\mathrm{p}}(\mathcal{S}\mathbf{u} + \mathbf{f})(\mathbf{x}) + \mathcal{B}_{\mathrm{p}}(\mathcal{T}\mathbf{u} + \mathbf{g})(\mathbf{x}) = \mathcal{A}(\mathcal{S}\mathbf{u} + \mathbf{f})(\mathbf{x}) + \mathcal{B}(\mathcal{T}\mathbf{u} + \mathbf{g})(\mathbf{x}) = \mathbf{u}(\mathbf{x}).$$

The last equality is due to the fact that $\mathbf{u}$ solves (24). Now since $\mathbf{v}|_{B_\rho} = \mathbf{u}$ we obtain from (29) that

$$\mathbf{v} = \mathcal{A}_{\mathrm{p}}(\mathcal{S}\mathbf{v} + \mathbf{f}) + \mathcal{B}_{\mathrm{p}}(\mathcal{T}\mathbf{v} + \mathbf{g}),$$

which means that $\mathbf{v}$ is a solution to the periodic integro-differential equation (28).

Now, for $\mathbf{f} = \mathbf{g} = 0$, since (24) has a unique solution, we have $\mathbf{u} = 0$ in $H(\mathrm{curl}\,, B_\rho)$. Then from (29) $\mathbf{v} = \mathcal{A}_{\mathrm{p}}(\mathcal{S}\mathbf{u}) + \mathcal{B}_{\mathrm{p}}(\mathcal{T}\mathbf{u}) = 0$, which means that (28) also has a unique solution. □

Next we prove that the operator $I - \mathcal{A}_{\mathrm{p}}\mathcal{S} - \mathcal{B}_{\mathrm{p}}\mathcal{T}$ from (28) satisfies a Gårding inequality in $H_{\mathrm{p}}(\mathrm{curl}\,, \Omega_R)$. This proof is similar to that of theorem 4.4 in [30]. We present a short proof here for the convenience of the readers.

Theorem 8. *Suppose that assumption 1 and (20) hold true. Then there exists a positive constant C and a compact operator L on* $H_{\mathrm{p}}(\mathrm{curl}\,, \Omega_R)$ *such that*

$$\mathrm{Re}\,(\mathbf{u}-\mathcal{A}_{\mathrm{p}}\mathcal{S}\mathbf{u}-\mathcal{B}_{\mathrm{p}}\mathcal{T}\mathbf{u},\mathbf{u})_{k,H_{\mathrm{p}}(\mathrm{curl}\,,\Omega_R)}\geqslant C\|\mathbf{u}\|^2_{k,H_{\mathrm{p}}(\mathrm{curl}\,,\Omega_R)}-\mathrm{Re}\,(L\mathbf{u},\mathbf{u})_{k,H_{\mathrm{p}}(\mathrm{curl}\,,\Omega_R)},\tag{30}$$

for all $\mathbf{u}\in H_{\mathrm{p}}(\mathrm{curl}\,,\Omega_R)$.

Proof. We can write the left-hand side of (30) as

$$(\mathbf{u}-\mathcal{A}_{\mathrm{p}}\mathcal{S}\mathbf{u}-\mathcal{B}_{\mathrm{p}}\mathcal{T}\mathbf{u},\mathbf{u})_{k,H_{\mathrm{p}}(\mathrm{curl}\,,\Omega_R)}=(\mathbf{u}-\mathcal{A}\mathcal{S}\mathbf{u}-\mathcal{B}\mathcal{T}\mathbf{u},\mathbf{u})_{k,H(\mathrm{curl}\,,B_{2\rho})}\tag{31}$$

$$-(\mathcal{A}_{\mathrm{p}}\mathcal{S}\mathbf{u}+\mathcal{B}_{\mathrm{p}}\mathcal{T}\mathbf{u},\mathbf{u})_{k,H(\mathrm{curl}\,,\Omega_R\setminus B_{2\rho})}\tag{32}$$

$$+\|\mathbf{u}\|^2_{k,H(\mathrm{curl}\,,\Omega_R\setminus B_{2\rho})}.\tag{33}$$

The Garding inequality of the first term in (31) is already proved in theorem 8. The second term can be written as a compact term. We define $L_1 : H_{\mathrm{p}}(\mathrm{curl}\,,\Omega_R)\to H_{\mathrm{p}}(\mathrm{curl}\,,\Omega_R)$ as

$$(L_1\mathbf{u},\mathbf{u})_{k,H_{\mathrm{p}}(\mathrm{curl}\,,\Omega_R)}=(\mathcal{A}_{\mathrm{p}}\mathcal{S}\mathbf{u}+\mathcal{B}_{\mathrm{p}}\mathcal{T}\mathbf{u},\mathbf{u})_{k,H(\mathrm{curl}\,,\Omega_R\setminus B_{2\rho})}.$$

Since the kernel $\mathcal{K}$ is a smooth function on $\Omega\times\Omega_R\setminus B_{2\rho}$, the volume potential mapping $\mathbf{g}$ to $\int_{\Omega_R}\mathcal{K}(\mathbf{x},\mathbf{y})\mathbf{g}(\mathbf{y})\mathrm{d}\mathbf{y}$ is a compact operator from $L^2(\Omega)^3$ to $H^2(\Omega_R\setminus B_{2\rho})^3$. Recall that $\mathcal{S},\mathcal{T}:H_{\mathrm{p}}(\mathrm{curl}\,,\Omega_R)\to L^2(\Omega)^3$ are bounded operators. From these facts it is deduced that $\mathcal{A}_{\mathrm{p}}\mathcal{S}$ and $\mathcal{B}_{\mathrm{p}}\mathcal{T}$ are compact operators from $H_{\mathrm{p}}(\mathrm{curl}\,,\Omega_R)$ to $H(\mathrm{curl}\,,\Omega_R\setminus B_{2\rho})$. Therefore, let $\mathbf{u}_n$ be a sequence which converges weakly to zero in $H_{\mathrm{p}}(\mathrm{curl}\,,\Omega_R)$. Using standard arguments we can prove that $L_1\mathbf{u}_n$ converges strongly to zero in $H_{\mathrm{p}}(\mathrm{curl}\,,\Omega_R)$, see e.g. [30]. □

We now study a spectral Galerkin approximation for the periodic integral equation (28). For $N\in\mathbb{N}$ we consider a finite dimensional subspace of $H_{\mathrm{p}}(\mathrm{curl}\,,\Omega_R)$ as

$$\mathbf{T}_N:=(\mathrm{span}\{\phi_{\mathbf{j}}:\mathbf{j}\in\mathbb{Z}^3_N\})^3,\quad \mathbb{Z}^3_N:=\{\mathbf{j}\in\mathbb{Z}^3:-N/2<j_{1,2,3}\leqslant N/2\},$$

where $\phi_{\mathbf{j}}\in L^2(\Omega_R)$ are the trigonometric basis functions in (26). Note that the union $\cup_{N\in\mathbb{N}}\mathbf{T}_N$ is dense in $H_{\mathrm{p}}(\mathrm{curl}\,,\Omega_R)$. Now we consider the following finite dimensional problem. Given $\mathbf{f},\mathbf{g}\in L^2(\Omega_R)^3$, find $\mathbf{u}_N\in\mathbf{T}_N$ such that

$$(\mathbf{u}_N-\mathcal{A}_{\mathrm{p}}\mathcal{S}\mathbf{u}_N-\mathcal{B}_{\mathrm{p}}\mathcal{T}\mathbf{u}_N,\mathbf{v}_N)_{H_{\mathrm{p}}(\mathrm{curl}\,,\Omega_R)}=(\mathcal{A}_{\mathrm{p}}\mathbf{f}+\mathcal{B}_{\mathrm{p}}\mathbf{g},\mathbf{v}_N)_{H_{\mathrm{p}}(\mathrm{curl}\,,\Omega_R)}\tag{34}$$

for all $\mathbf{v}_N\in\mathbf{T}_N$.

Thanks to the Gårding inequality of the periodic equation (28) we have the following standard quasi-optimal convergence result for problem (34), see, e.g. [38, theorem 4.2.9].

Theorem 9. *Suppose that assumption 1 and (20) hold true. Let* $\mathbf{u}\in H_{\mathrm{p}}(\mathrm{curl}\,,\Omega_R)$ *be the unique solution of (28). Then there is* $N_0\in\mathbb{N}$ *such that the finite-dimensional problem (34) has a unique solution* $\mathbf{u}_N$ *for all* $N\geqslant N_0$. *In this case,*

$$\|\mathbf{u}_N-\mathbf{u}\|_{H_{\mathrm{p}}(\mathrm{curl}\,,\Omega_R)}\leqslant C\inf_{\mathbf{v}_N\in\mathbf{T}_N}\|\mathbf{v}_N-\mathbf{u}\|_{H_{\mathrm{p}}(\mathrm{curl}\,,\Omega_R)},$$

with a constant C *independent of* $\mathbf{u}$, $\mathbf{u}_N$ *and* $N\geqslant N_0$.

We remark that if the coefficients ε_{r}, μ_{r} and ξ are L^∞-functions, solution $\mathbf{u}$ may not be more regular than $H(\mathrm{curl}\,)$. Therefore, it is probably not possible to improve the estimate above in theorem 9, see also [2] for a similar situation. We can have more regularity on the solution by assuming the global smoothness of ε_{r}, μ_{r} and ξ. It is important to note that the volume

potential with the periodic smooth kernel $\mathcal{K}$ is diagonalized by the trigonometric basis $\{\phi_{\mathbf{j}}\}$, which means

$$\int_{\Omega_R} \mathcal{K}(\mathbf{x},\cdot)\phi_{\mathbf{j}}\,\mathrm{d}\mathbf{y} = \sqrt{8R^3}\,\widehat{\mathcal{K}}(\mathbf{j})\phi_{\mathbf{j}}(\mathbf{x}) \quad \text{for all } \mathbf{j}\in\mathbb{Z}^3,$$

where $\widehat{\mathcal{K}}(\mathbf{j}) = \int_{\Omega_R}\mathcal{K}(\mathbf{z})\overline{\phi_{\mathbf{j}}(\mathbf{z})}\mathrm{d}\mathbf{z}$. This leads to the fact that the orthogonal projection $\mathcal{P}_N : H_{\mathrm{p}}(\mathrm{curl}\,,\Omega_R)\to\mathbf{T}_N$ defined by

$$\mathcal{P}_N(\mathbf{v}) = \sum_{j\in\mathbb{Z}_N^3}\widehat{\mathbf{v}}(\mathbf{j})\phi_{\mathbf{j}},$$

commutes with the periodic (convolution) operators $\mathcal{A}_{\mathrm{p}}$, $\mathcal{B}_{\mathrm{p}}$. Therefore, the finite-dimensional problem (34) can be rewritten as follows. Find $\mathbf{u}_N\in\mathbf{T}_N$ such that

$$\mathbf{u}_N - \mathcal{A}_{\mathrm{p}}(\mathcal{P}_N(\mathcal{S}\mathbf{u}_N)) - \mathcal{B}_{\mathrm{p}}(\mathcal{P}_N(\mathcal{T}\mathbf{u}_N)) = \mathcal{A}_{\mathrm{p}}(\mathcal{P}_N\mathbf{f}) + \mathcal{B}_{\mathrm{p}}(\mathcal{P}_N\mathbf{g}). \tag{35}$$

We can discretize this equation in a spectral domain, which means we look for the Fourier coefficients of $\mathbf{u}_N$. The Fourier coefficients of $\mathcal{A}_{\mathrm{p}}\mathbf{v}_N$ and $\mathcal{B}_{\mathrm{p}}\mathbf{v}_N$ for $\mathbf{v}_N\in\mathbf{T}_N$ can be computed thanks to the fact that the integrals have a convolution structure and that the Fourier coefficients of kernel $\mathcal{K}$ can be explicitly computed as

$$\widehat{\mathcal{K}}(\mathbf{j}) = \frac{1}{\sqrt{8R^3}}\sum_{\mathbf{n}\in\mathbb{Z}_N^3}\widehat{\Phi}_{\mathrm{p}}(\mathbf{n})\widehat{\psi}(\mathbf{j}-\mathbf{n}), \quad \mathbf{j}\in\mathbb{Z}^3,$$

where $\widehat{\Phi}_{\mathrm{p}}(\mathbf{n})$ are the Fourier coefficients of the periodic kernel without smoothing. They have explicit formulas: for $\pi^2|\mathbf{n}|^2\neq R^2k^2$,

$$\widehat{\Phi}_{\mathrm{p}}(\mathbf{n}) = \begin{cases} \frac{1}{k^2\sqrt{8R^3}}(\mathrm{e}^{\mathrm{i}kR}(1-\mathrm{i}kR)-1) & |\mathbf{n}|=0 \\ \frac{R^2}{\sqrt{8R^3}(\pi^2|\mathbf{n}|^2-R^2k^2)}(1-\mathrm{e}^{\mathrm{i}kR}\cos(\pi|\mathbf{n}|)-\frac{\mathrm{i}kR}{\pi|\mathbf{n}|}\mathrm{e}^{\mathrm{i}kR}\sin(\pi|\mathbf{n}|)), & |\mathbf{n}|\neq 0. \end{cases}$$

Otherwise $\widehat{\Phi}_{\mathrm{p}}(\mathbf{n}) = -\mathrm{i}R/(4k\sqrt{R^3})(1-\mathrm{e}^{\mathrm{i}kR}\sin(kR)/(kR))$. Since ψ is a smooth function, its Fourier coefficients decay rapidly, that is, a short truncation in the series in $\widehat{\mathcal{K}}(\mathbf{j})$ converges rapidly to the exact value. These facts are crucially exploited for fast methods (e.g. fast Fourier transforms) for solving the discrete version of (35). We refer to [30] for more details about the numerical implementation and other aspects of the method.

5.1. Numerical examples for the direct solver

We present in this section some numerical examples examining the performance of the direct solver for the case of smoothly varying coefficients, discontinuous coefficients, and wave numbers $k=1$ and $k=30$. The simulations were carried out on a Quad Core 3.6 GHz machine with 32GB RAM. In all examples the tolerance for the GMRES solver for the linear system obtained from discretizing (35) is chosen to be 10^{-8}. For $r>0$ let $\mathbf{h}$ be a smoothly varying function defined by

$$\mathbf{h}(\mathbf{x},r) = r\exp\left(1-\frac{r^2}{r^2-|\mathbf{x}|^2}\right), \quad \mathbf{x}\in\mathbb{R}^3,$$

and consider the following diagonal matrices

Table 1. Performance of the direct solver for smoothly varying coefficients and $k = 1$.

N	$\max_{\widehat{\mathbf{x}}}\{\lvert\mathbf{u}^{\infty}(\widehat{\mathbf{x}})\rvert\}$	Time (s)
32	0.136 834 74	1.7
64	0.136 956 17	16.2
128	0.136 956 10	137.4

Table 2. Performance of the direct solver for smoothly varying coefficients and $k = 30$.

N	$\max_{\widehat{\mathbf{x}}}\{\lvert\mathbf{u}^{\infty}(\widehat{\mathbf{x}})\rvert\}$	Time (s)
32	0.375 069 73	4.0
64	0.372 226 26	26.6
128	0.372 221 22	218.2

$$A_{\varepsilon} = \begin{bmatrix} 2.4 & 0 & 0 \\ 0 & 2.5 & 0 \\ 0 & 0 & 2.2 \end{bmatrix}, \quad A_{\mu} = \begin{bmatrix} 2.1 & 0 & 0 \\ 0 & 2.3 & 0 \\ 0 & 0 & 2.2 \end{bmatrix}, \quad A_{\xi} = \begin{bmatrix} 0.01 & 0 & 0 \\ 0 & 0.02 & 0 \\ 0 & 0 & 0.05 \end{bmatrix}.$$

5.2. Example 1 (smoothly varying coefficients)

In this example we consider matrix-valued functions $\varepsilon_{\mathrm{r}}, \mu_{\mathrm{r}}^{-1}, \xi$ that are smoothly varying functions as

$$\varepsilon_{\mathrm{r}} = \begin{cases} A_{\varepsilon}\mathbf{h}(\mathbf{x}, r) + I_3, & |\mathbf{x}| < r \\ I_3, & \text{else} \end{cases}, \quad \mu_{\mathrm{r}}^{-1} = \begin{cases} A_{\mu}\mathbf{h}(\mathbf{x}, r) + I_3, & |\mathbf{x}| < r \\ I_3, & \text{else} \end{cases}, \quad \xi = \begin{cases} A_{\xi}\mathbf{h}(\mathbf{x}, r), & |\mathbf{x}| < r \\ 0, & \text{else.} \end{cases}$$

Here we choose $r = 1$ for $k = 1$ and $r = 0.5$ for $k = 30$. The eigenvalues of A_{ξ} are small because ξ is assumed to be 'small' in assumption 1. N is the number of discrete points in each dimension of the computational domain. Using lemma 10 the far-field pattern $\mathbf{u}^{\infty}(\widehat{\mathbf{x}})$ is evaluated at 900 points uniformly distributed on the unit sphere. Time in the tables means the computation time for the direct solver. Our computer is out of memory for $N = 150$, showing that the solver is very efficient for the case of smooth coefficients for bi-anisotropic scattering media. Indeed, we can observe a fast convergence in tables 1 and 2 for both smaller and larger wave numbers. We also remark that for the case of smooth coefficients, the performance of the method can be improved by using a two-grid (or multigrid) method instead of GMRES for solving the linear system (see, e.g. [16]).

5.3. Example 2 (discontinuous coefficients)

Let $B_r = \{|\mathbf{x}| < r\}$. For any 3×3 matrix M we define a discontinuous function F as

$$F(\mathbf{x}; M) = \begin{cases} \frac{1}{2}M + I_3 & \mathbf{x} \in (-\frac{r}{4}, \frac{r}{4})^3 \\ M\mathbf{h}(\mathbf{x}, r) + I_3 & B_r \setminus (-\frac{r}{4}, \frac{r}{4})^3 \\ I_3, & \text{else.} \end{cases}$$

We consider in this example matrix-valued functions $\varepsilon_{\mathrm{r}}, \mu_{\mathrm{r}}^{-1}, \xi$ that are functions with discontinuities as

Table 3. Performance of the direct solver for discontinuous coefficients and $k = 1$.

N	$\max_{\widehat{\mathbf{x}}}\{\lvert\mathbf{u}^\infty(\widehat{\mathbf{x}})\rvert\}$	Time (s)
32	0.134 276 39	1.5
64	0.132 864 91	15.64
128	0.132 049 13	136.8

Table 4. Performance of the direct solver for discontinuous coefficients and $k = 30$.

N	$\max_{\widehat{\mathbf{x}}}\{\lvert\mathbf{u}^\infty(\widehat{\mathbf{x}})\rvert\}$	Time (s)
32	0.374 164 40	3.7
64	0.370 998 17	26.9
128	0.370 658 24	235

$$\varepsilon_{\mathrm{r}} = F(\mathbf{x}; A_\varepsilon), \quad \mu_{\mathrm{r}}^{-1} = F(\mathbf{x}; A_\mu), \quad \xi = \begin{cases} \frac{1}{2}A_\xi & \mathbf{x} \in (-\frac{r}{4}, \frac{r}{4})^3 \\ A_\xi \mathbf{h}(\mathbf{x}, r) & B_r \setminus (-\frac{r}{4}, \frac{r}{4})^3 \\ 0, & \text{else.} \end{cases} \tag{36}$$

As in the case of smooth coefficients we choose $r = 1$ for $k = 1$ and $r = 0.5$ for $k = 30$. Although the convergence can be seen again in tables 3 and 4, the performance of the direct solver in this case is not as good as that of the case of smooth coefficients. This is reasonable because the order of convergence is lower due to the lack of regularity of the solution that is commented on after theorem 9. It is also not clear whether multigrid methods can be applied to improve the performance of the solver in this case where we have discontinuous matrix-valued coefficients.

6. Orthogonality sampling methods for inverse scattering problems

We consider the inverse scattering problems of recovering the bi-anisotropic medium from both the far-field pattern data and the scattered field data. These data are generated by one or a few incident fields. We will extend the orthogonality sampling method introduced by Potthast in [35] for sound-soft acoustic scattering to our case of electromagnetic scattering from bi-anisotropic media. The main advantages of this sampling method are that it is robust to noise, computationally cheap and requires data for only one or a few incident fields. We first study the case of far-field pattern data. It is well known that the scattered electric field $\mathbf{u}$ has the asymptotic form

$$\mathbf{u}(\mathbf{x}) = \frac{\mathrm{e}^{\mathrm{i}k|\mathbf{x}|}}{|\mathbf{x}|}\left(\mathbf{u}^\infty(\widehat{\mathbf{x}}) + O\left(\frac{1}{|\mathbf{x}|}\right)\right), \quad |\mathbf{x}| \to \infty,$$

uniformly in all directions $\widehat{\mathbf{x}} = \mathbf{x}/|\mathbf{x}| \in \mathbb{S}^2$. The function $\mathbf{u}^\infty(\widehat{\mathbf{x}})$ defined on the unit sphere $\mathbb{S}^2$ is called the electric far-field pattern.

We need the following lemma for our analysis.

Lemma 10. *The electric far-field pattern* $\mathbf{u}^\infty(\widehat{\mathbf{x}})$ *satisfies*

$$\mathbf{u}^\infty(\widehat{\mathbf{x}}) = k^2 \int_\Omega \frac{\mathrm{e}^{-\mathrm{i}k\widehat{\mathbf{x}}\cdot\mathbf{y}}}{4\pi}\widehat{\mathbf{x}} \times (\mathcal{S}\mathbf{E}(\mathbf{y}) \times \widehat{\mathbf{x}})\mathrm{d}\mathbf{y} + \mathrm{i}k \int_\Omega \frac{\mathrm{e}^{-\mathrm{i}k\widehat{\mathbf{x}}\cdot\mathbf{y}}}{4\pi}\widehat{\mathbf{x}} \times \mathcal{T}\mathbf{E}(\mathbf{y})\mathrm{d}\mathbf{y},$$

where $\mathbf{E} = \mathbf{u} + \mathbf{E}_{\text{in}}$ *is the total electric field in (4).*

Proof. The asymptotic behavior of $\Phi(\mathbf{x}, \mathbf{y})$ for $|\mathbf{x}| \to \infty$ is well known

$$\Phi(\mathbf{x}, \mathbf{y}) = \frac{\mathrm{e}^{\mathrm{i}k|\mathbf{x}|}}{|\mathbf{x}|}\left(\frac{\mathrm{e}^{-\mathrm{i}k\widehat{\mathbf{x}}\cdot\mathbf{y}}}{4\pi} + O\left(\frac{1}{|\mathbf{x}|}\right)\right).$$

In addition, for any $\mathbf{a} \in \mathbb{C}^3$, we have from [12, theorem 6.9] that

$$\operatorname{curl}_{\mathbf{x}}(\Phi(\mathbf{x}, \mathbf{y})\mathbf{a}) = \mathrm{i}k\frac{\mathrm{e}^{\mathrm{i}k|\mathbf{x}|}}{|\mathbf{x}|}\left(\frac{\mathrm{e}^{-\mathrm{i}k\widehat{\mathbf{x}}\cdot\mathbf{y}}}{4\pi}\widehat{\mathbf{x}} \times \mathbf{a} + O\left(\frac{|\mathbf{a}|}{|\mathbf{x}|}\right)\right), \tag{37}$$

$$\operatorname{curl}_{\mathbf{x}}\operatorname{curl}_{\mathbf{x}}(\Phi(\mathbf{x}, \mathbf{y})\mathbf{a}) = k^2\frac{\mathrm{e}^{\mathrm{i}k|\mathbf{x}|}}{|\mathbf{x}|}\left(\frac{\mathrm{e}^{-\mathrm{i}k\widehat{\mathbf{x}}\cdot\mathbf{y}}}{4\pi}\widehat{\mathbf{x}} \times (\mathbf{a} \times \widehat{\mathbf{x}}) + O\left(\frac{|\mathbf{a}|}{|\mathbf{x}|}\right)\right). \tag{38}$$

Since we are interested in $\mathbf{u}(\mathbf{x})$ for $|\mathbf{x}| \to \infty$, using (37), (38) and the fact $k^2\Phi(\mathbf{x}, \mathbf{y}) = -\Delta\Phi(\mathbf{x}, \mathbf{y})$ for $\mathbf{x} \neq \mathbf{y}$, and the identity $-\Delta + \nabla\operatorname{div} = \operatorname{curl}\operatorname{curl}$, we obtain that

$$\begin{aligned}
\mathbf{u}(\mathbf{x}) &= (k^2 + \nabla\operatorname{div})\int_\Omega \Phi(\mathbf{x}, \mathbf{y})\mathcal{S}\mathbf{E}(\mathbf{y})\,\mathrm{d}\mathbf{y} + \operatorname{curl}\int_\Omega \Phi(\mathbf{x}, \mathbf{y})\mathcal{T}\mathbf{E}(\mathbf{y})\,\mathrm{d}\mathbf{y},\\
&= \int_\Omega \operatorname{curl}_{\mathbf{x}}\operatorname{curl}_{\mathbf{x}}(\Phi(\mathbf{x}, \mathbf{y})\mathcal{S}\mathbf{E}(\mathbf{y}))\,\mathrm{d}\mathbf{y} + \int_\Omega \operatorname{curl}_{\mathbf{x}}(\Phi(\mathbf{x}, \mathbf{y})\mathcal{T}\mathbf{E}(\mathbf{y}))\,\mathrm{d}\mathbf{y},\\
&= \frac{\mathrm{e}^{\mathrm{i}k|\mathbf{x}|}}{|\mathbf{x}|}\left(k^2\int_\Omega \frac{\mathrm{e}^{-\mathrm{i}k\widehat{\mathbf{x}}\cdot\mathbf{y}}}{4\pi}\widehat{\mathbf{x}} \times (\mathcal{S}\mathbf{E}(\mathbf{y}) \times \widehat{\mathbf{x}})\,\mathrm{d}\mathbf{y} + \mathrm{i}k\int_\Omega \frac{\mathrm{e}^{-\mathrm{i}k\widehat{\mathbf{x}}\cdot\mathbf{y}}}{4\pi}\widehat{\mathbf{x}} \times \mathcal{T}\mathbf{E}(\mathbf{y})\,\mathrm{d}\mathbf{y} + O\left(\frac{1}{|\mathbf{x}|}\right)\right).
\end{aligned}$$

The last equation means that the far-field $\mathbf{u}^\infty$ satisfies the desired property of the lemma. □

6.1. Imaging with far-field pattern data

We are interested in imaging of the scatterer Ω given the far-field pattern $\mathbf{u}^\infty(\widehat{\mathbf{x}})$, for all $\widehat{\mathbf{z}} \in \mathbb{S}^2$, generated by one or a few incident plane waves. Let $\mathbf{y}_s$ be the sampling points in the imaging process and $\mathbf{p} \in \mathbb{R}^3$ be some polarization vector. We define the imaging functional I_{far} as

$$I_{\text{far}}(\mathbf{y}_s) := \left|\int_{\mathbb{S}^2} \mathbf{u}^\infty(\widehat{\mathbf{x}}) \cdot (\mathbf{p}\overline{\Phi^\infty(\widehat{\mathbf{x}}, \mathbf{y}_s)})\,\mathrm{d}s(\widehat{\mathbf{x}})\right|. \tag{39}$$

Here $\Phi^\infty(\widehat{\mathbf{x}}, \mathbf{y}) = \mathrm{e}^{-\mathrm{i}k\widehat{\mathbf{x}}\cdot\mathbf{y}}/(4\pi)$ is the far-field pattern of $\Phi(\mathbf{x}, \mathbf{y})$. We show in the next lemma that this functional $I_{\text{far}}(\mathbf{y}_s)$ must be close to zero when sampling points $\mathbf{y}_s$ are away from Ω, and it takes finite values when $\mathbf{y}_s$ approaches points $\mathbf{y}$ of Ω. This behavior thus would allow us to be able to recover geometrical information (e.g. location, shape) of the scatterer Ω.

Lemma 11. *The functional* I_{far} *defined in (39) satisfies*

$$I_{\text{far}}(\mathbf{y}_s) = \left|\frac{\mathbf{p}}{16\pi^2} \cdot \int_\Omega \mathbf{U}(\mathbf{y} - \mathbf{y}_s, \mathcal{T}\mathbf{E}(\mathbf{y})) + \mathbf{V}(\mathbf{y} - \mathbf{y}_s, \mathcal{S}\mathbf{E}(\mathbf{y}))\mathrm{d}\mathbf{y}\right|,$$

where $\mathbf{U}, \mathbf{V} : \mathbb{R}^3 \times \mathbb{C}^3 \to \mathbb{C}^3$ *are bounded functions with explicit formulae (see in the proof), which satisfy the following limits (pointwise in* $\mathbf{a}$*)*

$$\lim_{|\mathbf{z}|\to 0}\mathbf{U}(\mathbf{z},\mathbf{a})=0,\quad \lim_{|\mathbf{z}|\to\infty}\mathbf{U}(\mathbf{z},\mathbf{a})=0,$$
$$\lim_{|\mathbf{z}|\to 0}\mathbf{V}(\mathbf{z},\mathbf{a})=k^2(1,1,1)^\top,\quad \lim_{|\mathbf{z}|\to\infty}\mathbf{V}(\mathbf{z},\mathbf{a})=0.$$

Proof. We have the well-known Funk–Hecke formula as follows (see, e.g. [12])

$$\int_{\mathbb{S}^2}\mathrm{e}^{-\mathrm{i}k\widehat{\mathbf{x}}\cdot\mathbf{z}}Y_n(\widehat{\mathbf{x}})\mathrm{d}s(\widehat{\mathbf{x}})=4\pi j_n(k|\mathbf{z}|)Y_n(\widehat{\mathbf{z}}),\quad n=0,1,2\ldots,$$

where j_n are Bessel functions of order n and Y_n are spherical harmonics of order n. Let $n=0$ in the Funk–Hecke formula, and for any $\mathbf{a}\in\mathbb{C}^3$ we have

$$\begin{aligned}&\int_{\mathbb{S}^2}\mathrm{curl}_{\,\mathbf{z}}(\mathrm{e}^{-\mathrm{i}k\mathbf{z}\cdot\widehat{\mathbf{x}}}\mathbf{a})\mathrm{d}s(\widehat{\mathbf{x}})=-\mathrm{i}k\int_{\mathbb{S}^2}(\widehat{\mathbf{x}}\times\mathbf{a})\,\mathrm{e}^{-\mathrm{i}k\mathbf{z}\cdot\widehat{\mathbf{x}}}\mathrm{d}s(\widehat{\mathbf{x}})\\&=\mathbf{U}(\mathbf{z},\mathbf{a}):=4\pi k\widehat{\mathbf{z}}\times\mathbf{a}\left(\frac{\cos(k|\mathbf{z}|)}{k|\mathbf{z}|}-\frac{j_0(k|\mathbf{z}|)}{k|\mathbf{z}|}\right),\\&\int_{\mathbb{S}^2}\mathrm{curl}_{\,\mathbf{z}}\mathrm{curl}_{\,\mathbf{z}}(\mathrm{e}^{-\mathrm{i}k\mathbf{z}\cdot\widehat{\mathbf{x}}}\mathbf{a})\mathrm{d}s(\widehat{\mathbf{x}})=-k^2\int_{\mathbb{S}^2}\widehat{\mathbf{x}}\times(\mathbf{a}\times\widehat{\mathbf{x}})\mathrm{e}^{-\mathrm{i}k\mathbf{z}\cdot\widehat{\mathbf{x}}}\mathrm{d}s(\widehat{\mathbf{x}})\\&=\begin{pmatrix}a_1\left[\partial^2_{1,1}j_0(k|\mathbf{z}|)-\Delta j_0(k|\mathbf{z}|)\right]+a_2\partial^2_{2,1}j_0(k|\mathbf{z}|)+a_3\partial^2_{3,1}j_0(k|\mathbf{z}|)\\a_1\partial^2_{1,2}j_0(k|\mathbf{z}|)+a_2\left[\partial^2_{2,2}j_0(k|\mathbf{z}|)-\Delta j_0(k|\mathbf{z}|)\right]+a_3\partial^2_{3,2}j_0(k|\mathbf{z}|)\\a_1\partial^2_{1,3}j_0(k|\mathbf{z}|)+a_2\partial^2_{2,3}j_0(k|\mathbf{z}|)+a_3\left[\partial^2_{3,3}j_0(k|\mathbf{z}|)-\Delta j_0(k|\mathbf{z}|)\right]\end{pmatrix},\end{aligned}\tag{40}$$

where

$$\partial^2_{m,n}j_0(k|\mathbf{z}|)=\frac{\partial^2 j_0(k|\mathbf{z}|)}{\partial z_m\partial z_n},\quad m,n=1,2,3.$$

Using the fact that $\Delta j_0(k|\mathbf{z}|)=-k^2j_0(k|\mathbf{z}|)$ and some calculations lead to

$$-k^2\int_{\mathbb{S}^2}\widehat{\mathbf{x}}\times(\mathbf{a}\times\widehat{\mathbf{x}})\mathrm{e}^{-\mathrm{i}k\mathbf{z}\cdot\widehat{\mathbf{x}}}\mathrm{d}s(\widehat{\mathbf{x}})=\mathbf{V}(\mathbf{z},\mathbf{a})=\begin{pmatrix}V_1(\mathbf{z},\mathbf{a})\\V_2(\mathbf{z},\mathbf{a})\\V_3(\mathbf{z},\mathbf{a})\end{pmatrix}\tag{41}$$

where

$$V_j(\mathbf{z},\mathbf{a})=k^2\left(\frac{|\mathbf{z}|^2-(\mathbf{a}\cdot\mathbf{z})z_j}{|\mathbf{z}|^2}\right)j_0(k|\mathbf{z}|)-3\left(\frac{(\mathbf{a}\cdot\mathbf{z})z_j}{|\mathbf{z}|^4}\right)(\cos(k|\mathbf{z}|)-j_0(k|\mathbf{z}|)),\quad j=1,2,3.$$

It is important to note that function $V_j(\mathbf{z},\mathbf{a})$ tends to k^2 and $\mathbf{U}(\mathbf{z},\mathbf{a})$ tends to zero as $|\mathbf{z}|$ tends to zero. Indeed, this can be seen by rewriting $V_j(\mathbf{z},\mathbf{a})$ and $\mathbf{U}(\mathbf{z},\mathbf{a})$ as

$$V_j(\mathbf{z},\mathbf{a})=k^2j_0(k|\mathbf{z}|)-\frac{(\mathbf{a}\cdot\mathbf{z})z_j}{|\mathbf{z}|^2}\left(k^2j_0(k|\mathbf{z}|)+3k^2\frac{\cos(k|\mathbf{z}|)-j_0(k|\mathbf{z}|)}{k^2|\mathbf{z}|^2}\right),\tag{42}$$

$$\mathbf{U}(\mathbf{z},\mathbf{a})=4\pi k^2(\mathbf{z}\times\mathbf{a})\left(\frac{\cos(k|\mathbf{z}|)-j_0(k|\mathbf{z}|)}{k^2|\mathbf{z}|^2}\right),\tag{43}$$

and by using the following

$$\left|\frac{(\mathbf{a}\cdot\mathbf{z})z_j}{|\mathbf{z}|^2}\right| \leqslant C(\mathbf{a}), \quad \lim_{|\mathbf{z}|\to 0} j_0(k|\mathbf{z}|) = 1, \quad \lim_{|\mathbf{z}|\to 0} \frac{\cos(k|\mathbf{z}|) - j_0(k|\mathbf{z}|)}{k^2|\mathbf{z}|^2} = -\frac{1}{3},$$

where $C(\mathbf{a})$ is a positive constant depending on $\mathbf{a}$. In fact $C(\mathbf{a})$ can be computed explicitly, for instance $C(\mathbf{a}) = \max\{2|a_1|, |a_2|/2, |a_3|/2\}$ for $j = 1$. Furthermore, it can be easily checked that functions $\mathbf{U}$ and $\mathbf{V}$ decay rapidly as $|\mathbf{z}|$ tends to infinity. More precisely,

$$\mathbf{U}(\mathbf{z},\mathbf{a}) = O\left(\frac{1}{|\mathbf{z}|}\right), \quad \mathbf{V}(\mathbf{z},\mathbf{a}) = O\left(\frac{1}{|\mathbf{z}|}\right), \quad |\mathbf{z}| \to \infty. \tag{44}$$

Now using lemma 10, (40) and (41) we compute the inner product

$$\begin{aligned}
\int_{\mathbb{S}^2} \mathbf{u}^\infty(\widehat{\mathbf{x}})\cdot(\mathbf{p}\overline{\Phi^\infty(\widehat{\mathbf{x}},\mathbf{y}_s)})\mathrm{d}s(\widehat{\mathbf{x}}) &= \int_{\mathbb{S}^2} k^2 \int_\Omega \frac{\mathrm{e}^{-\mathrm{i}k\widehat{\mathbf{x}}\cdot\mathbf{y}}}{4\pi}\widehat{\mathbf{x}}\times(\mathcal{S}\mathbf{E}(\mathbf{y})\times\widehat{\mathbf{x}})\,\mathrm{d}\mathbf{y}\cdot(\mathbf{p}\overline{\Phi^\infty(\widehat{\mathbf{x}},\mathbf{y}_s)})\mathrm{d}s(\widehat{\mathbf{x}}) \\
&\quad + \int_{\mathbb{S}^2} \mathrm{i}k \int_\Omega \frac{\mathrm{e}^{-\mathrm{i}k\widehat{\mathbf{x}}\cdot\mathbf{y}}}{4\pi}\widehat{\mathbf{x}}\times\mathcal{T}\mathbf{E}(\mathbf{y})\,\mathrm{d}\mathbf{y}\cdot(\mathbf{p}\overline{\Phi^\infty(\widehat{\mathbf{x}},\mathbf{y}_s)})\mathrm{d}s(\widehat{\mathbf{x}}) \\
&= \frac{k^2\mathbf{p}}{16\pi^2}\cdot\int_\Omega\int_{\mathbb{S}^2} \mathrm{e}^{-\mathrm{i}k\widehat{\mathbf{x}}\cdot(\mathbf{y}-\mathbf{y}_s)}\widehat{\mathbf{x}}\times(\mathcal{S}\mathbf{E}(\mathbf{y})\times\widehat{\mathbf{x}})\mathrm{d}s(\widehat{\mathbf{x}})\mathrm{d}\mathbf{y} \\
&\quad + \frac{\mathrm{i}k\mathbf{p}}{16\pi^2}\cdot\int_\Omega\int_{\mathbb{S}^2} \mathrm{e}^{-\mathrm{i}k\widehat{\mathbf{x}}\cdot(\mathbf{y}-\mathbf{y}_s)}\widehat{\mathbf{x}}\times\mathcal{T}\mathbf{E}(\mathbf{y})\mathrm{d}s(\widehat{\mathbf{x}})\mathrm{d}\mathbf{y} \\
&= -\frac{\mathbf{p}}{16\pi^2}\cdot\int_\Omega \mathbf{U}(\mathbf{y}-\mathbf{y}_s,\mathcal{T}\mathbf{E}(\mathbf{y})) + \mathbf{V}(\mathbf{y}-\mathbf{y}_s,\mathcal{S}\mathbf{E}(\mathbf{y}))\mathrm{d}\mathbf{y}.
\end{aligned}$$

This calculation together with the asymptotic behaviors of $\mathbf{U}$ and $\mathbf{V}$ established above finish the proof. □

The next theorem shows the stability of our imaging functional.

Theorem 12 (Stability estimate). *Let $|\mathbb{S}^2|$ be the surface area of $\mathbb{S}^2$ and $|\mathbf{p}|$ be the magnitude of $\mathbf{p}\in\mathbb{R}^3$. Define $I_{\mathrm{far},\delta}(\mathbf{x}) = (\mathbf{u}_\delta^\infty, \mathbf{p}\Phi^\infty(\cdot,\mathbf{x}))_{L^2(\mathbb{S}^2)^3}$. The imaging functional $I_{\mathrm{far}}(\cdot)$ defined in (39) for the far-field pattern $\mathbf{u}^\infty$ generated by an incident wave $\mathbf{E}_{\mathrm{in}}$ satisfies*

$$|I_{\mathrm{far}}(\mathbf{x}) - I_{\mathrm{far},\delta}(\mathbf{x})| \leqslant |\mathbf{p}|\,|\mathbb{S}^2|\|\mathbf{u}^\infty - \mathbf{u}_\delta^\infty\|_{L^2(\mathbb{S}^2)^3}, \quad \text{for all } \mathbf{x}\in\mathbb{R}^3.$$

Proof. The proof follows directly from the Cauchy–Schwarz inequality

$$\begin{aligned}
|I_{\mathrm{far}}(\mathbf{y}_s) - I_{\mathrm{far},\delta}(\mathbf{x})| &\leqslant \left|\int_{\mathbb{S}^2}(\mathbf{u}^\infty(\widehat{\mathbf{x}}) - \mathbf{u}_\delta^\infty(\widehat{\mathbf{x}}))\cdot(\mathbf{p}\overline{\Phi^\infty(\widehat{\mathbf{x}},\mathbf{y}_s)})\mathrm{d}s(\widehat{\mathbf{x}})\right| \\
&\leqslant |\mathbf{p}||\mathbb{S}^2|\|\mathbf{u}^\infty - \mathbf{u}_\delta^\infty\|_{L^2(\mathbb{S}^2)^3}.
\end{aligned}$$

□

6.2. Imaging with scattered field data

We are also interested in the imaging of the scatterer Ω from some boundary data of the scattered field $\mathbf{u}(\mathbf{x})$ instead of its far-field pattern. Again these data are generated by one or a few incident waves $\mathbf{E}_{\mathrm{in}}$. We will show how to construct the imaging functional. To this end we need a technical assumption on the global smoothness of coefficients P, Q and ξ.

Note that the imaging functional in this case provides an alternative choice for the imaging of Ω using the exact formula of the scattered field instead of its far-field pattern. This might be useful in the case where measurements are given in terms of the scattered field or one is uncertain about whether the far-field approximation is accurate enough. We first have the following lemma, which is important to the derivation of the imaging functional.

Lemma 13. *Assume that coefficients P, Q and ξ are globally smooth functions. The scattered field* $\mathbf{u}$ *satisfies*

$$\mathbf{u}(\mathbf{x}) = \int_\Omega \Phi(\mathbf{x},\cdot)\left[k^2\mathcal{S}\mathbf{E} + \nabla\mathrm{div}(\mathcal{S}\mathbf{E}) + \mathrm{curl}\,(\mathcal{T}\mathbf{E})\right]\mathrm{d}\mathbf{y}, \quad \mathbf{x}\in\mathbb{R}^3,$$

where $\mathbf{E}$ *is again the total electric field.*

Proof. Since P, Q and ξ are globally smooth functions, elliptic regularity results guarantee that $\mathcal{S}\mathbf{E}$ and $\mathcal{T}\mathbf{E}$ are also smooth functions with compact support in Ω. Using Green's theorem and the fact that

$$\frac{\partial\Phi(\mathbf{x},\mathbf{y})}{\partial x_j} = -\frac{\partial\Phi(\mathbf{x},\mathbf{y})}{\partial y_j}, \quad j=1,2,3,$$

we have

$$\begin{aligned}
\mathbf{u}(\mathbf{x}) &= (k^2+\nabla\mathrm{div})\int_\Omega \Phi(\mathbf{x},\mathbf{y})\mathcal{S}\mathbf{E}(\mathbf{y})\mathrm{d}\mathbf{y} + \mathrm{curl}\int_\Omega \Phi(\mathbf{x},\mathbf{y})\mathcal{T}\mathbf{E}(\mathbf{y})\mathrm{d}\mathbf{y},\\
&= \int_\Omega \Phi(\mathbf{x},\mathbf{y})k^2\mathcal{S}\mathbf{E}(\mathbf{y})\mathrm{d}\mathbf{y} + \int_\Omega \nabla_{\mathbf{x}}\mathrm{div}_{\mathbf{x}}\left[\Phi(\mathbf{x},\mathbf{y})\mathcal{S}\mathbf{E}(\mathbf{y})\right]\mathrm{d}\mathbf{y} + \int_\Omega \mathrm{curl}_{\,\mathbf{x}}\left[\Phi(\mathbf{x},\mathbf{y})\mathcal{T}\mathbf{E}(\mathbf{y})\right]\mathrm{d}\mathbf{y}\\
&= \int_\Omega \Phi(\mathbf{x},\mathbf{y})\left[k^2\mathcal{S}\mathbf{E}(\mathbf{y}) + \nabla\mathrm{div}(\mathcal{S}\mathbf{E}(\mathbf{y})) + \mathrm{curl}\,(\mathcal{T}\mathbf{E}(\mathbf{y}))\right]\mathrm{d}\mathbf{y}.
\end{aligned}$$

This completes the proof. □

Consider a ball B_r of radius r, centered at the origin, suppose that $\overline{\Omega}\subset B_r$ and that the scattered field data $\mathbf{u}(\mathbf{x})$ are given on ∂B_r for some radius r that is large enough. This also means that we measure at a distance that is far from the scatterer. We now consider the imaging functional

$$I(\mathbf{y}_s) := \left|\int_{\partial B_r} \mathbf{u}(\mathbf{x})\cdot\mathbf{p}\overline{\Phi(\mathbf{x},\mathbf{y}_s)}\,\mathrm{d}s(\mathbf{x})\right|, \tag{45}$$

where $\mathbf{y}_s$ and $\mathbf{p}\in\mathbb{R}^3$ are again sampling points and the polarization vector, respectively. We show in the next lemma that this functional allows us to image the scatterer Ω. For the convenience of the presentation, we set

$$\mathbf{w} = k^2\mathcal{S}\mathbf{E} + \nabla\mathrm{div}(\mathcal{S}\mathbf{E}) + \mathrm{curl}\,(\mathcal{T}\mathbf{E}),$$

which means $\mathbf{u}(\mathbf{x}) = \int_\Omega \Phi(\mathbf{x},\cdot)\mathbf{w}\mathrm{d}\mathbf{y}$.

Lemma 14. *The imaging functional I defined in (45) satisfies*

$$I(\mathbf{y}_s) = \frac{1}{4\pi k}\left|\int_\Omega j_0(k|\mathbf{y}_s-\mathbf{y}|)\mathbf{p}\cdot\mathbf{w}(\mathbf{y})\mathrm{d}\mathbf{y}\right|.$$

Proof. The proof relies on the well-known Helmholtz–Kirchhoff identity

$$\Phi(\mathbf{y}_s,\mathbf{y}) - \overline{\Phi(\mathbf{y}_s,\mathbf{y})} = 2ik\int_{\partial B_r}\Phi(\mathbf{y},\mathbf{x})\overline{\Phi(\mathbf{y}_s,\mathbf{x})}\,\mathrm{d}s(\mathbf{x}).$$

This identity can be proved using Green's theorems and the Sommerfeld radiation condition for $\Phi(\mathbf{x},\mathbf{y})$. The radiation condition can be used thanks to the assumption on the large radius r of B_r. We refer to [13, theorem 2.2] for a proof of the Helmholtz–Kirchhoff identity. Indeed, using this identity the inner product in the imaging functional I can be computed as

$$\begin{aligned}\int_{\partial B_r}\mathbf{u}(\mathbf{x})\cdot\mathbf{p}\overline{\Phi(\mathbf{x},\mathbf{y}_s)}\mathrm{d}s(\mathbf{x}) &= \int_{\partial B_r}\int_{\Omega}\Phi(\mathbf{x},\mathbf{y})\overline{\Phi(\mathbf{x},\mathbf{y}_s)}\,\mathbf{p}\cdot\mathbf{w}(\mathbf{y})\mathrm{d}\mathbf{y}\mathrm{d}s(\mathbf{x})\\ &= \int_{\Omega}\int_{\partial B_r}\Phi(\mathbf{y},\mathbf{x})\overline{\Phi(\mathbf{y}_s,\mathbf{x})}\mathrm{d}s(\mathbf{x})\mathbf{p}\cdot\mathbf{w}(\mathbf{y})\mathrm{d}\mathbf{y}\\ &= \int_{\Omega}\frac{\Phi(\mathbf{y}_s,\mathbf{y})-\overline{\Phi(\mathbf{y}_s,\mathbf{y})}}{2ik}\mathbf{p}\cdot\mathbf{w}(\mathbf{y})\mathrm{d}\mathbf{y}\\ &= \frac{1}{4\pi k}\int_{\Omega}j_0(k|\mathbf{y}_s-\mathbf{y}|)\mathbf{p}\cdot\mathbf{w}(\mathbf{y})\mathrm{d}\mathbf{y}.\end{aligned}$$

This completes the proof. □

The imaging functional I in this case is also as stable as that of the far-field pattern case. Since we assume that the radius r of B_r is large enough, it is sufficient to have the stability of I in the ball $B_{r'}$ for some $r' < r$. The proof again just follows from the Cauchy–Schwarz inequality.

Theorem 15 (Stability estimate). *Define* $I_\delta(\mathbf{x}) = (\mathbf{u}_\delta, \mathbf{p}\Phi(\cdot,\mathbf{x}))_{L^2(\partial B_r)^3}$. *The imaging functional* $I(\cdot)$ *defined in (45) for the scattered field data* $\mathbf{u}(\mathbf{x})$, $\mathbf{x}\in\partial B_r$, *generated by an incident wave* $\mathbf{E}_{\text{in}}$ *satisfies*

$$|I(\mathbf{x}) - I_\delta(\mathbf{x})| \leqslant |\mathbf{p}|\;||\Phi(\cdot,\cdot)||_{L^2(\partial B_r\times B_{r'})}\|\mathbf{u}-\mathbf{u}_\delta\|_{L^2(\partial B_r)^3}, \quad \text{for all } \mathbf{x}\in B_{r'}.$$

7. Numerical examples for the inverse problem

For the numerical examples in this section the scattering data are generated by the numerical solver studied in section 5. First, using the solver we obtain the numerical solution to the finite-dimensional problem (35) whose restriction on Ω is the numerical scattered field $\mathbf{u}$. Second, the far-field pattern data $\mathbf{u}^\infty(\widehat{\mathbf{x}})$ are calculated using the formula in lemma 10. We consider the far-field pattern data collected at 2500 points uniformly distributed on $\mathbb{S}^2$. Except the case of figure 5(d), these data, including all three components of the far-field, are generated by one incident plane wave propagating along the z-direction. We only present results for the imaging functional I_{far} for the far-field pattern data. The case of functional I with scattered field data provides similar results. We consider numerical examples for which the scattering objects are defined as in the following. First consider the matrices

$$A_\varepsilon = \begin{bmatrix}1.5 & 0 & 0\\ 0 & 1.4 & 0\\ 0 & 0 & 1.3\end{bmatrix},\quad A_\mu = \begin{bmatrix}1.1 & 0 & 0\\ 0 & 1.2 & 0\\ 0 & 0 & 1.3\end{bmatrix},\quad A_\xi = \begin{bmatrix}0.005 & 0 & 0\\ 0 & 0.004 & 0\\ 0 & 0 & 0.003\end{bmatrix},$$

and the smooth function

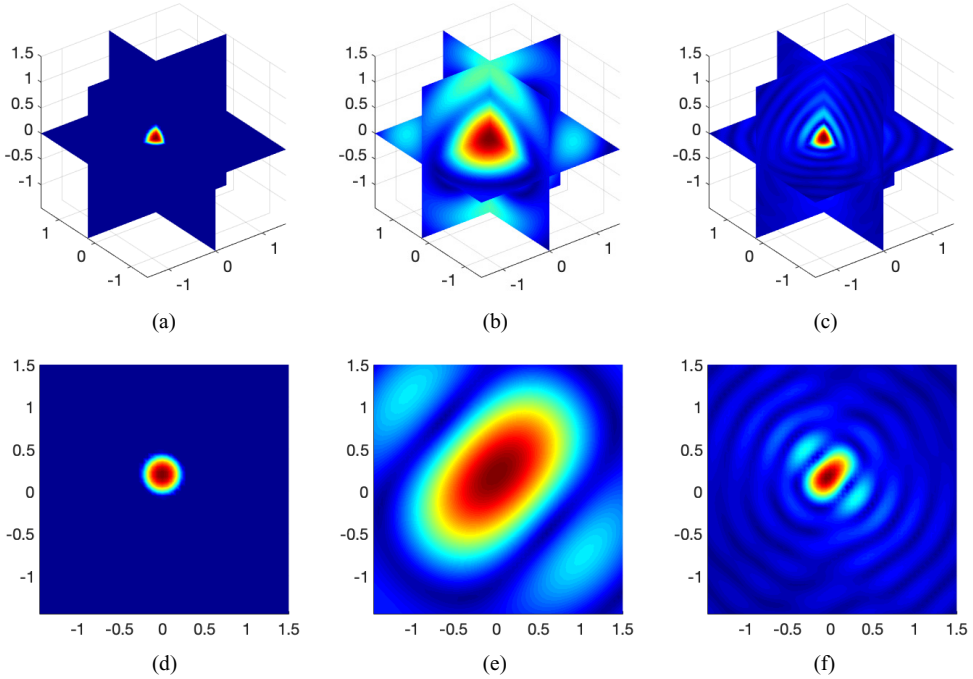

Figure 2. Reconstruction results for different wave numbers for a scattering ball with smoothly varying coefficients defined in (46). Noiseless data associated with one incident plane wave direction $(0,0,1)^\top$ are used for the pictures. (a) Exact profile. (b) $k = 3$. (c) $k = 10$. (d) Top view of (a). (e) Top view of (b). (f) Top view of (c).

$$\mathbf{h}(\mathbf{x},\mathbf{a},r) = r\exp\left(1 - \frac{r^2}{r^2 - |\mathbf{x}-\mathbf{a}|^2}\right), \quad \mathbf{x} \in \mathbb{R}^3.$$

Let $B(\mathbf{a},r)$ be the ball centered at $\mathbf{a}$ with radius r. In the first two examples (figures 2 and 3) the anisotropic scatterers are characterized by smooth coefficients given by

$$\varepsilon_{\mathrm{r}} = \begin{cases} A_\varepsilon \mathbf{h}(\mathbf{x},\mathbf{a},r) + I_3, & \mathbf{x} \in B(\mathbf{a},r) \\ I_3, & \text{else} \end{cases}, \quad \mu_{\mathrm{r}}^{-1} = \begin{cases} A_\mu \mathbf{h}(\mathbf{x},\mathbf{a},r) + I_3, & \mathbf{x} \in B(\mathbf{a},r) \\ I_3, & \text{else} \end{cases},$$
$$\xi = \begin{cases} A_\xi \mathbf{h}(\mathbf{x},\mathbf{a},r), & \mathbf{x} \in B(\mathbf{a},r) \\ 0, & \text{else} \end{cases}, \tag{46}$$

where

$$\mathbf{a} = (0, 0.2, 0)^\top, \quad r = 0.3.$$

In the third example (figure 4), the coefficients for the three scattering balls are given by

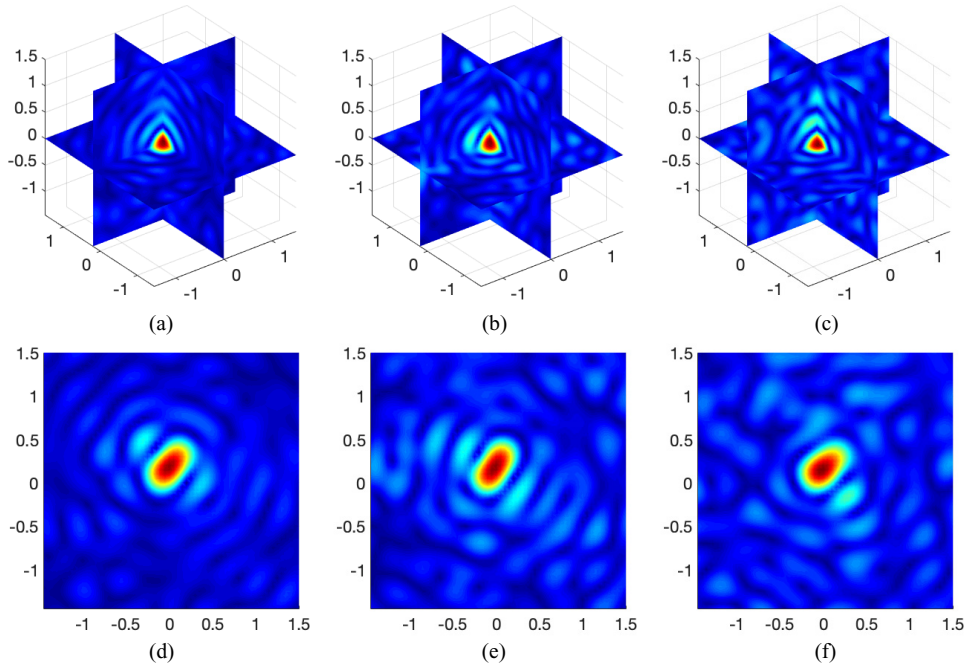

Figure 3. Reconstruction results for the scattering ball in figure 2(a) from noisy data associated with one incident plane wave direction $(0,0,1)^\top$. (a) 30% noise, $k=10$. (b) 60% noise, $k=10$. (c) 80% noise, $k=10$. (d) Top view of (a). (e) Top view of (b). (f) Top view of (c).

$$\varepsilon_{\mathrm{r}}=\begin{cases}A_\varepsilon\mathbf{h}(\mathbf{x},\mathbf{a},r_1)+I_3, & \mathbf{x}\in B(\mathbf{a},r_1)\\ A_\varepsilon\mathbf{h}(\mathbf{x},\mathbf{b},r_2)+I_3, & \mathbf{x}\in B(\mathbf{b},r_2)\\ A_\varepsilon\mathbf{h}(\mathbf{x},\mathbf{c},r_3)+I_3, & \mathbf{x}\in B(\mathbf{c},r_3)\\ I_3, & \text{else}\end{cases},\quad \mu_{\mathrm{r}}^{-1}=\begin{cases}A_\mu\mathbf{h}(\mathbf{x},\mathbf{a},r_1)+I_3, & \mathbf{x}\in B(\mathbf{a},r_1)\\ A_\mu\mathbf{h}(\mathbf{x},\mathbf{b},r_2)+I_3, & \mathbf{x}\in B(\mathbf{b},r_2)\\ A_\mu\mathbf{h}(\mathbf{x},\mathbf{c},r_3)+I_3, & \mathbf{x}\in B(\mathbf{c},r_3)\\ I_3, & \text{else}\end{cases},$$
$$\xi=\begin{cases}A_\xi\mathbf{h}(\mathbf{x},\mathbf{a},r_1), & \mathbf{x}\in B(\mathbf{a},r_1)\\ A_\xi\mathbf{h}(\mathbf{x},\mathbf{b},r_2), & \mathbf{x}\in B(\mathbf{b},r_2)\\ A_\xi\mathbf{h}(\mathbf{x},\mathbf{c},r_3), & \mathbf{x}\in B(\mathbf{c},r_3)\\ 0, & \text{else}\end{cases}, \tag{47}$$

where

$$\mathbf{a}=(0.2,0,0)^\top,\quad \mathbf{b}=(-0.4,0,0)^\top,\quad \mathbf{c}=(0.6,-0.7,0)^\top,$$
$$r_1=0.3,\quad r_2=0.2,\quad r_3=0.25.$$

The scattering object in the last example (figure 5) is characterized by discontinuous coefficients defined by

$$\varepsilon_{\mathrm{r}}=\begin{cases}A_\varepsilon+I_3, & \mathbf{x}\in\Omega\\ I_3, & \text{else}\end{cases},\quad \mu_{\mathrm{r}}^{-1}=\begin{cases}A_\mu+I_3, & \mathbf{x}\in\Omega\\ I_3, & \text{else}\end{cases},$$
$$\xi=\begin{cases}A_\xi, & \mathbf{x}\in\Omega\\ 0, & \text{else}\end{cases}, \tag{48}$$

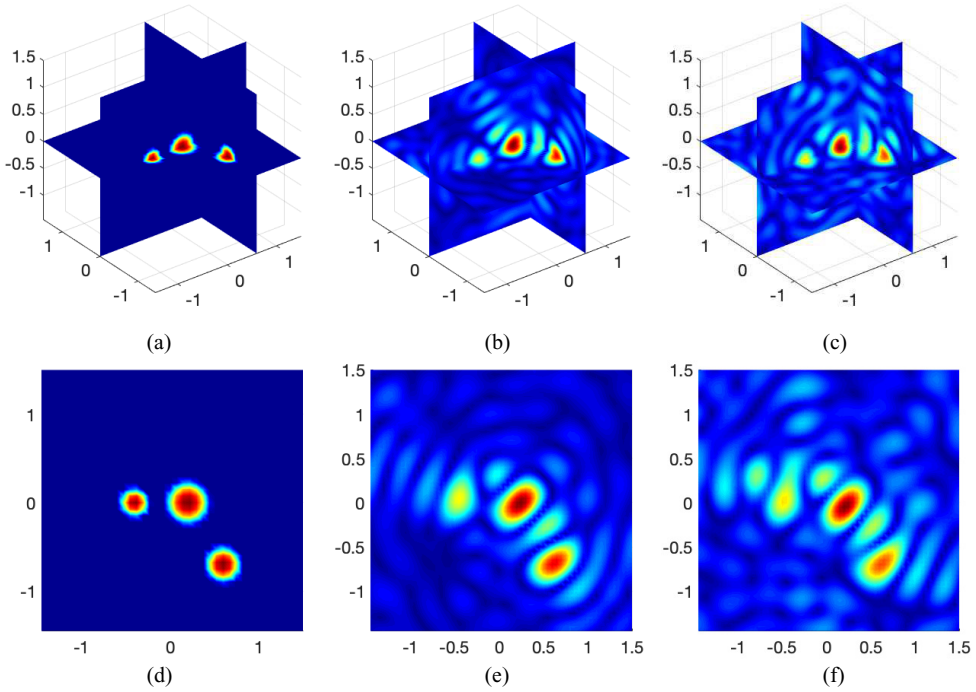

Figure 4. Reconstruction results for three different scattering balls (defined in (47)) from noisy data associated with one incident plane wave direction $(0, 0, 1)^\top$. (a) Exact profile. (b) 30% noise, $k = 10$. (c) 60% noise, $k = 10$. (d) Top view of (a). (e) Top view of (b). (f) Top view of (c).

where

$$\Omega = \{x_1^2 + x_2^2 \leqslant 0.4^2, |x_3| \leqslant 0.7\} \cup \{x_2^2 + x_3^2 \leqslant 0.4^2, |x_1| \leqslant 0.7\} \cup \{x_1^2 + x_3^2 \leqslant 0.4^2, |x_2| \leqslant 0.7\}.$$

Figure 2 shows the dependence of the reconstruction on the wave number k for noiseless data. For $k = 10$ the wavelength is approximately 0.6 which is also the diameter of the scatterer. The result in this case is therefore better than that of the case $k = 3$. We can see that for $k = 10$ the geometry (particularly the location) of the scatterer is well reconstructed in this case. With the same scattering object as in the first experiment presented in figure 2, we show in the second numerical experiment (see figure 3) that the imaging functional is robust with respect to noise in the far-field data. The noise we consider here is an additive noise. More precisely, the scattering data are added by a complex-valued noise matrix containing random numbers that are uniformly distributed on $(-1, 1)$. The numerical reconstructions (even with multiple numbers of experiments) are still quite reasonable with different levels of noise (30%, 60% and 80%). This robustness can be justified by the stability estimates for the imaging functional in our theory.

Figure 4 indicates that the imaging functional is also able to image multiple scattering balls from noisy data. The geometry of the scattering balls is again well reconstructed even with the presence of high amounts of additive noise in the data (30% and 60%). The resolution for the reconstructed images in this case is also quite good for wave number $k = 10$. We note that unlike in the case of only one scattering ball (figure 3) the reconstructions for three scattering

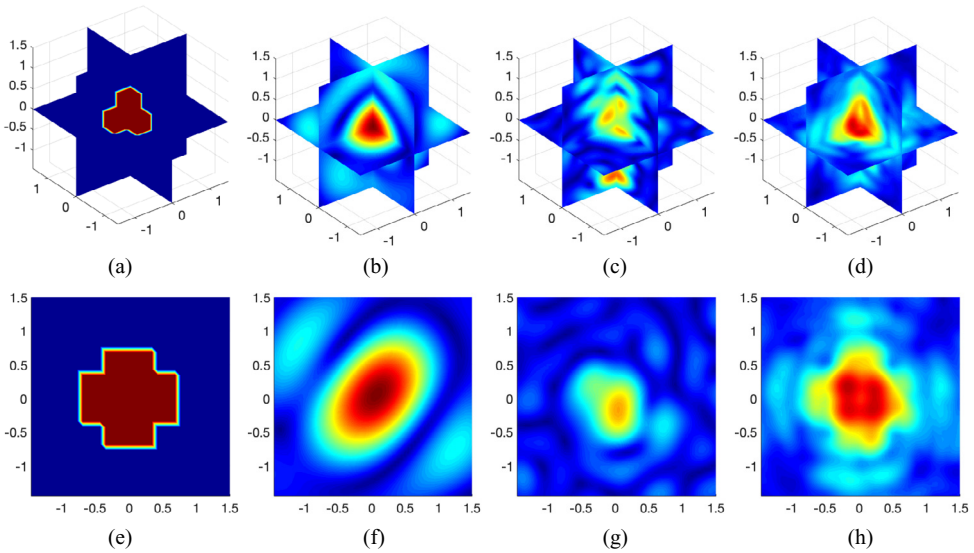

Figure 5. Reconstruction results from noisy data (30% noise) for an extended scattering object defined in (48). One incident plane wave direction $(0,0,1)^\top$ is used in pictures (b) and (c), while six incident plane wave directions $(\pm1,0,0)^\top, (0,\pm1,0)^\top, (0,0,\pm1)^\top$ are used for picture (d). (a) Exact profile. (b) $k=3$. (c) $k=7$. (d) $k=7$, six incident waves. (e) Top view of (a). (f) Top view of (b). (g) Top view of (c). (h) Top view of (d).

balls in this case are no longer reasonable with higher amounts of noise in the data. However, the imaging functional proposed does not seem to work well for extended scatterers although it may be able to locate these scatterers using lower frequencies, see figures 5(b) and (c). In other words, although the reconstructions are still quite robust to noise, the imaging functional may not be able to recover the shape of these extended scatterers; see also [35] for a similar situation in the scalar case of the OSM. We can improve the shape reconstruction by using multiple directions of incident plane waves, see figure 5(d). Following the suggestions in [35] one can integrate the imaging functional with respect to the directions of the incident plane. More precisely, here we use six incident directions $(\pm1,0,0)^\top, (0,\pm1,0)^\top, (0,0,\pm1)^\top$ for the incident plane waves and add the corresponding imaging functionals together. However, we do not yet have a theoretical justification for this use of multiple incident directions. For the scalar case, we refer to [24] to justify using multiple incident directions for an imaging functional that shares similar features to that of the OSM.

Acknowledgments

This work was partially supported by NSF grant DMS-1812693 and the Faculty Enhancement Program Award from Kansas State University.

ORCID iDs

Dinh-Liem Nguyen https://orcid.org/0000-0003-1580-4661

References

[1] Ammari H and Bao G 2003 Maxwell's equations in periodic chiral structures *Math. Nachr.* **251** 3–18

[2] Ammari H and Bao G 2008 Coupling of the finite element and boundary element methods for the scattering by periodic chiral structures *J. Comput. Math.* **26** 261–83

[3] Ammari H, Hamdache K and Nédélec J C 1999 Chirality in the Maxwell equations by the dipole approximation *SIAM J. Appl. Math.* **59** 2045–59

[4] Athanasiadis C, Costakis G and Stratis I G 2000 Electromagnetic scattering by a homogeneous chiral obstacle in a chiral environment *IMA J. Appl. Math.* **64** 245–58

[5] Athanasiadis C and Kardasi E 2008 Inverse electromagnetic scattering by a perfect conductor in a chiral environment *J. Inverse Ill-Posed Problems* **16** 1–18

[6] Athanasiadis C and Stratis I G 1998 Uniqueness of the inverse scattering problem by a chiral obstacle *Int. J. Appl. Electromagn. Mech.* **9** 123–33

[7] Boutet de Monvel A and Shepelsky D 1997 Direct and inverse scattering problem for a stratified nonreciprocal chiral medium *Inverse Problems* **13** 239

[8] Boutet de Monvel A and Shepelsky D 2000 A frequency-domain inverse problem for a dispersive stratified chiral medium *J. Math. Phys.* **41** 6116–29

[9] Cakoni F, Colton D and Monk P 2011 *The Linear Sampling Method in Inverse Electromagnetic Scattering* (Philadelphia, PA: SIAM)

[10] Ciarlet P Jr and Legendre G 2007 Well-posedness of the Drude–Born–Fedorov model for chiral media *Math. Models Methods Appl. Sci.* **17** 461

[11] Cocquet P H, Mazet P A and Mouysset V 2011 On well-posedness of some homogenized Drude–Born–Fedorov systems on a bounded domain and applications to metamaterials *C. R. Math.* **349** 99–103

[12] Colton D and Kress R 2013 *Inverse Acoustic and Electromagnetic Scattering Theory* 3rd edn (New York: Springer)

[13] Garnier J and Papanicolaou G 2016 *Passive Imaging with Ambient Noise* (Cambridge: Cambridge University Press)

[14] Gerlach T 1999 The two-dimensional electromagnetic inverse scattering problem for chiral media *Inverse Problems* **15** 1663

[15] Heumann S 2012 The factorization method for inverse scattering from chiral media *PhD Thesis* Karlsruher Institut für Technologie

[16] Hohage T 2006 Fast numerical solution of the electromagnetic medium scattering problem and applications to the inverse problem *J. Comput. Phys.* **214** 224–38

[17] Ito K, Jin B and Zou J 2012 A direct sampling method to an inverse medium scattering problem *Inverse Problems* **28** 025003

[18] Kirsch A 2007 An integral equation approach and the interior transmission problem for Maxwell's equations *Inverse Problems Imaging* **1** 159–80

[19] Kirsch A and Grinberg N 2008 *The Factorization Method for Inverse Problems* (*Oxford Lecture Series in Mathematics and its Applications* vol 36) (Oxford: Oxford University Press)

[20] Kong J A 1990 *Electromagnetic Wave Theory* 2nd edn (New York: Wiley-Interscience)

[21] Kriegler C E, Rill M S, Linden S and Wegener M 2010 Bianisotropic photonic metamaterials *IEEE J. Sel. Top. Quantum Electron.* **16** 367–75

[22] Li J and Zou J 2013 A direct sampling method for inverse scattering using far-field data *Inverse Problems Imaging* **7** 757–75

[23] Li S 2005 An inverse problem for Maxwell's equations in bi-isotropic media *SIAM J. Math. Anal.* **37** 1027–43

[24] Liu X 2017 A novel sampling method for multiple multiscale targets from scattering amplitudes at a fixed frequency *Inverse Problems* **33** 085011

[25] Mackay T G and Lakhtakia A 2010 *Electromagnetic Anisotropy and Bi-Anisotropy: a Field Guide* (Singapore: World Scientific)

[26] Marqués R, Medina F and Rafii-El-Idrissi R 2002 Role of bianisotropy in negative permeability and left-handed metamaterials *Phys. Rev.* B **65** 144440

[27] McDowall S R 1997 Boundary determination of material parameters from electromagnetic boundary information *Inverse Problems* **13** 153–63

[28] McDowall S R 2000 An electromagnetic inverse problem in chiral media *Trans. Am. Math. Soc.* **352** 2993–3013
[29] Nguyen D L 2016 The Factorization method for the Drude–Born–Fedorov model for periodic chiral structures *Inverse Problems Imaging* **10** 519–47
[30] Nguyen D L, Nguyen T N and Tran M P 2017 A Galerkin approximation for integro-differential equations in electromagnetic scattering from a chiral medium *Appl. Anal.* **96** 159–72
[31] Nicaise S 2013 Time domain study of the Drude–Born–Fedorov model for a class of heterogeneous chiral materials *Math. Methods Appl. Sci.* **36** 794–813
[32] Ola P 1994 Boundary integral equations for the scattering of electromagnetic waves by a homogeneous chiral obstacle *J. Math. Phys.* **35** 3969–80
[33] Pendry J 2004 A chiral route to negative refraction *Science* **19** 1353–5
[34] Potthast R 2006 A survey on sampling and probe methods for inverse problems *Inverse Problems* **22** R1–47
[35] Potthast R 2010 A study on orthogonality sampling *Inverse Problems* **26** 074015
[36] Potthast R and Stratis I G 2003 On the domain derivative for scattering by impenetrable obstacles in chiral media *IMA J. Appl. Math.* **68** 621–35
[37] Roach G F, Stratis I G and Yannacopoulos A N 2012 *Mathematical Analysis of Deterministic and Stochastic Problems in Complex Media Electromagnetics* (*Princeton Series in Applied Mathematics*) (Princeton, NJ: Princeton University Press)
[38] Sauter S and Schwab C 2007 *Boundary Element Methods* (Berlin: Springer)
[39] Stratis I G 1999 Electromagnetic scattering problems in chiral media: a review *Electromagnetics* **19** 547–62
[40] Wang Z and Guo R 2019 *A posteriori* error analysis for the scattering by obstacles in a homogeneous chiral environment *Appl. Numer. Math.* **135** 246–63
[41] Zhang D, Guo Y, Gong C and Wang G 2012 Numerical analysis for the scattering by obstacles in a homogeneous chiral environment *Adv. Comput. Math.* **36** 3–20